JRC Scientific and Technical Reports

On Plastic Collapse Analysis of KBS-3 Canister Mock-Up

Oliver Martin, Karl-Fredrik Nilsson and Nikola Jakšić

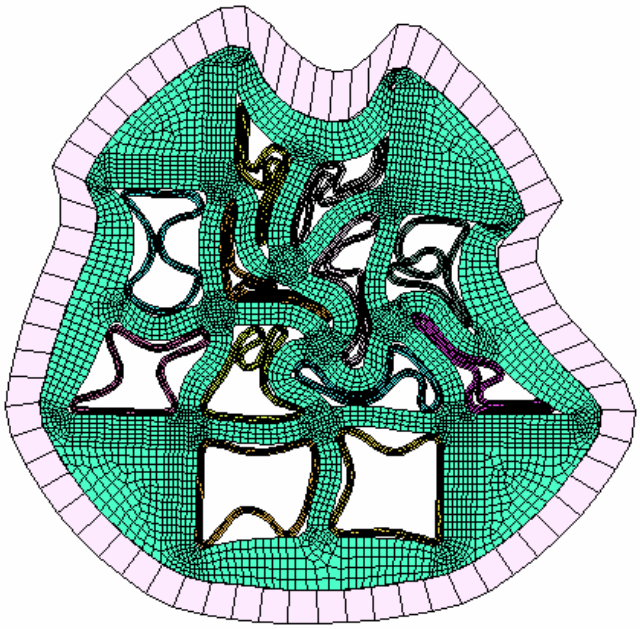

EUR 23224 EN - 2007

JRC EUROPEAN COMMISSION

Institute for Energy

The Institute for Energy provides scientific and technical support for the conception, development, implementation and monitoring of community policies related to energy. Special emphasis is given to the security of energy supply and to sustainable and safe energy production.

European Commission
Joint Research Centre
Institute for Energy

Contact information
Address: P.O. Box 1755 ZG, Petten
E-mail: oliver.martin@jrc.nl
Tel.: +31 224 56 5375
Fax: +31 224 56 5641

http://ie.jrc.ec.europa.eu/
http://www.jrc.ec.europa.eu/

Legal Notice
Neither the European Commission nor any person acting on behalf of the Commission is responsible for the use which might be made of this publication.

Europe Direct is a service to help you find answers to your questions about the European Union

Freephone number (*):

00 800 6 7 8 9 10 11

(*) Certain mobile telephone operators do not allow access to 00 800 numbers or these calls may be billed.

A great deal of additional information on the European Union is available on the Internet.
It can be accessed through the Europa server http://europa.eu/

JRC 41828

EUR 23224 EN
ISSN 1018-5593

Luxembourg: Office for Official Publications of the European Communities

© European Communities, 2007

Reproduction is authorised provided the source is acknowledged

Printed in The Netherlands

Content

Abstract

This report describes an in-depth finite element simulation of a spent fuel canister for geological disposal loaded in iso-static pressure until plastic collapse. The canister consists of a copper overpack and a ductile cast iron insert with steel cassettes where the spent fuel is placed. The higgly non-linear finite element analysis is based on the explicit formulation and includes large deformations, non-linear material behaviour and contact between the canister components. The analysis includes comparison between two-and three dimensional models and assessment of the different geometrical features such as corner radius of the cassette, cassette off-set, different bonding/dedonding conditions between insert and steel cassette. The analysis shows that the bonding cassette/insert has a large impact on the collapse load. Two large-scale mock-ups test that had been performed earlier are also simulated by the developed finite element models. There is a very good agreement between measured and computed deformations versus applied load and collapse load.

1. Introduction

The KBS-3 copper/cast iron canisters, Figure 1, are being developed in Scandinavia for geological disposal of spent nuclear fuel in crystalline rock [1],[2],[3]. The copper protects the canister from corrosion whereas the ductile cast iron insert provides the mechanical strength and eliminates the risk for criticality. The insert is cast around a steel cassette that provides the channels where the spent fuel is placed. The canister will be placed in shafts in a crystalline rock formation at a depth of 500 – 700 meters and surrounded by bentonite clay, Figure 2. The system needs to ensure that the level of radiotoxicity from the disposed spent nuclear fuel is negligible compared to the natural background dose. It will take more than 100,000 years before the spent fuel's radiotoxicity has decreased to the level of the natural uranium ore for which it was originally made. The canisters are therefore designed to contain the radionuclides for these time scales. This design life is longer than any other engineered products and features such as climate change need to be taken into account; in Scandinavia this means that ice-ages need to be considered and it has been estimated that the isostatic pressure during an ice-age can be up to 45 MPa.

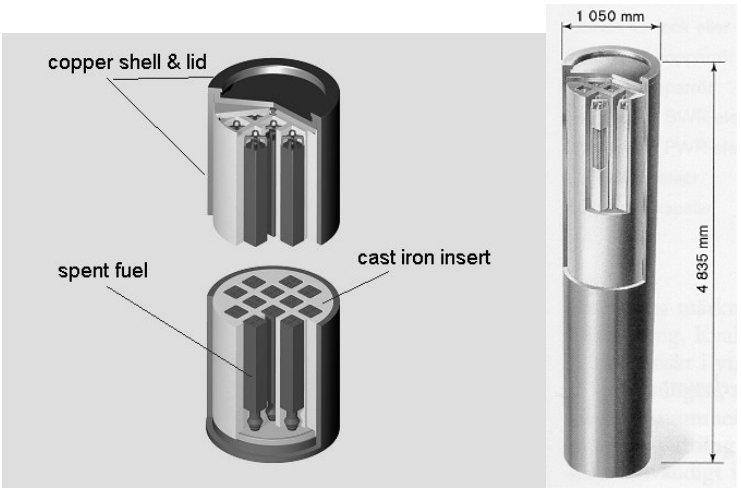

Figure 1: The KBS-3 spent fuel canister

A recent three-year research project demonstrated that the probability for mechanical failure of the canister at this load was extremely low [4],[5],[6]. To demonstrate the safety margins, verification tests were performed on two KBS-3 mock-ups that were loaded in a cold isostatic press to 132 and 139 MPa respectively. Thus the safety factor for the pressure load is at least a factor 3 [7], [8]. When the three-year project was reviewed the regulators stressed the importance of modelling the plastic collapse for overall confidence of the results. A simple plane strain finite element plastic collapse analysis had been performed with two-dimensional plane strain model and a quarter of the canister modelled assuming double symmetry conditions [6]. To get more confidence in predicting the failure and to understand the influence of different design parameters, more elaborate collapse models are needed. This report describes a finite element analysis where two and three-dimensional analyses are performed. The analysis also includes sensitivity study with respect to mesh density and relevant geometry features that had been idenfied as important such as cassette corner radius, bonding between cassette and insert and cassette off-set.

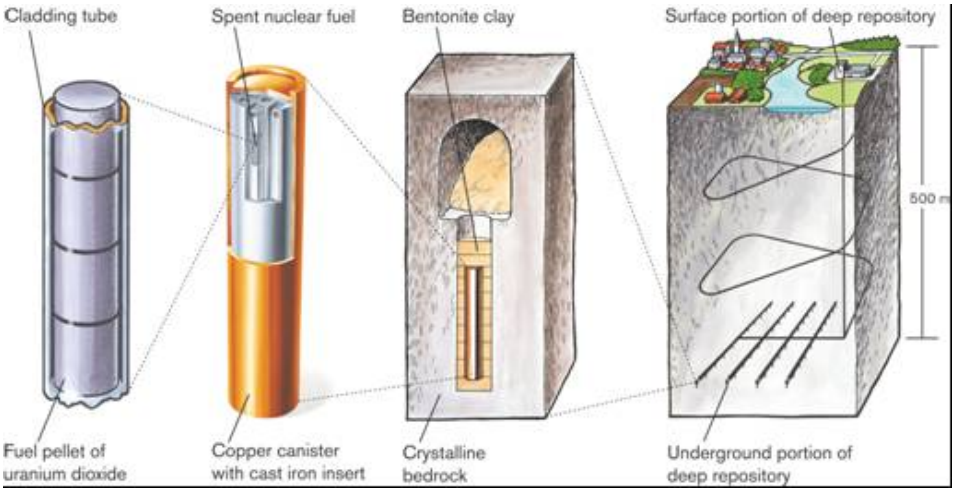

Figure 2: The KBS-3 system for geological disposal of spent nuclear fuel in crystalline rock

2. Design of the Mock-ups

Two canisters were used for the mock-up tests. The mock-ups have only a length of 1 m because of weight restrictions of the pressure test equipment. Figure 3a shows the mock-up before assembly and Figure 3b the assembled Mock-up 1 before the compression test.

Figure 3: a) Parts of the Mock-up 1 before assembly b) assembled Mock-up 1

Figure 4 illustrates the parts of the mock-up and how they are assembeld. The mock-ups are made from the following parts [7], [8]:

- Inserts of length 700 mm and of diameter 948 mm, cut from two different KBS-3 canister inserts (referred to as I24 and I26). The inserts have twelve almost quadratic shaped channels, each containing a square steel cassette with a thickness of 10 mm with inner dimensions of 160 × 160 respectively.
- Copper tube with inner diameter 952 mm, length 948 mm and wall thickness 50 mm.
- Two copper lids.
- Two steel plates of 48 mm thickness positioned between insert and lid at each end.

The KBS-3 canister has a length of almost five meters and the lids are welded to the copper tube. The bottom part of the insert has no fuel channels making the ends of the canister relatively stiff. Since the mock-ups are much shorter than the KBS-3 canisters the “stiffening effects” at the ends would be much larger if the same design were used for the ends. So to achieve more “flexible end effects” and to allow disassembly of the mock-ups after test, the lids were connected with bolts and O-rings to the insert [8].

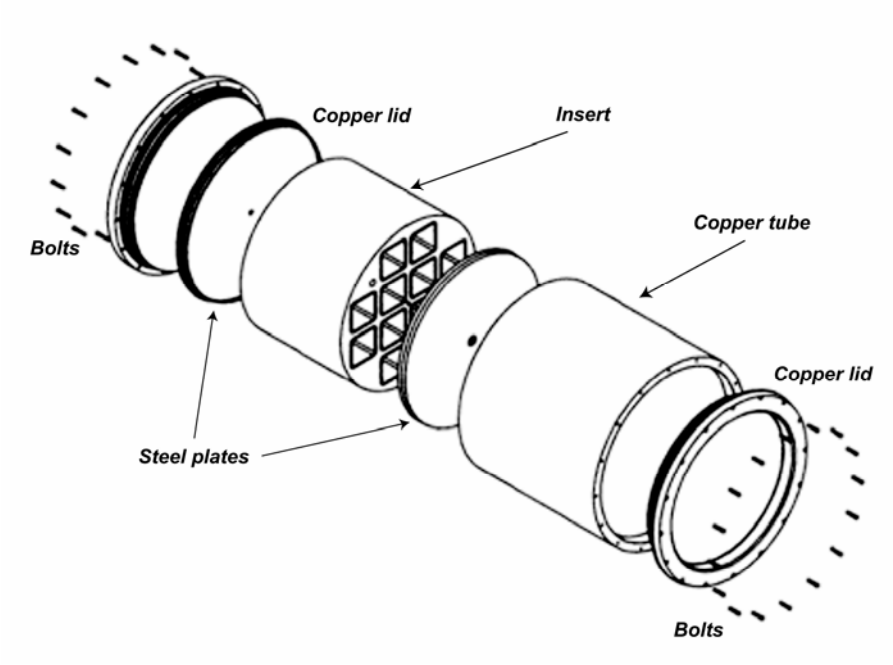

Figure 4: The different part of the mock-ups

The insert of Mock-up 1 was taken from an insert referred to as I26, for which the fuel channels have an offset of 12 mm from the full symmetric position. As a result the wall thickness between the corner of the fuel channels and the outer surface varies from 22 to 44 mm (see Figure 5). This offset leads to asymmetric load distributions with higher local stresses and higher deformations at the thinner side. In previous probabilistic analyses the offset has been identified as the most important factor for increasing the probability of canister failure at the design load of 44 MPa.

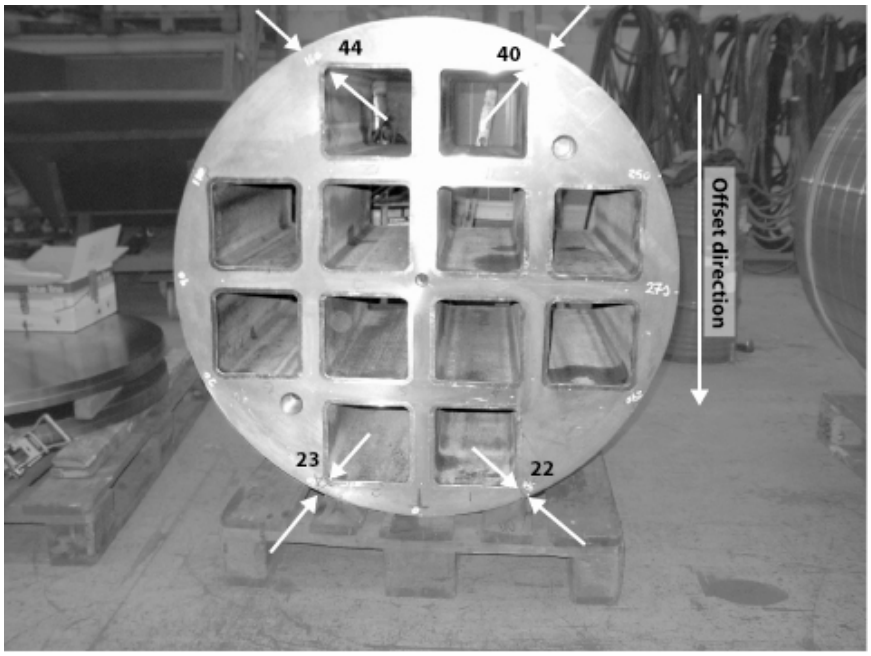

Figure 5: Cross section of insert I26

The insert for Mock-up 2 was taken from an insert referred to as I24, which has no channel offset, but where the corner radius of the steel cassettes was smaller (corner radius: 10-15 mm for I24 and 20-25 mm for I26). A smaller corner radius gives a higher stress concentration and lower failure load, but this effect on the computed probability for failure at the design load is much smaller than for the offset [4],[5],[6]. Stress-strain curves were measured for both inserts [9]; insert I26 is stiffer than insert I24 (see Figure 6). Ductile cast iron has also more hardening in compression than in tension.

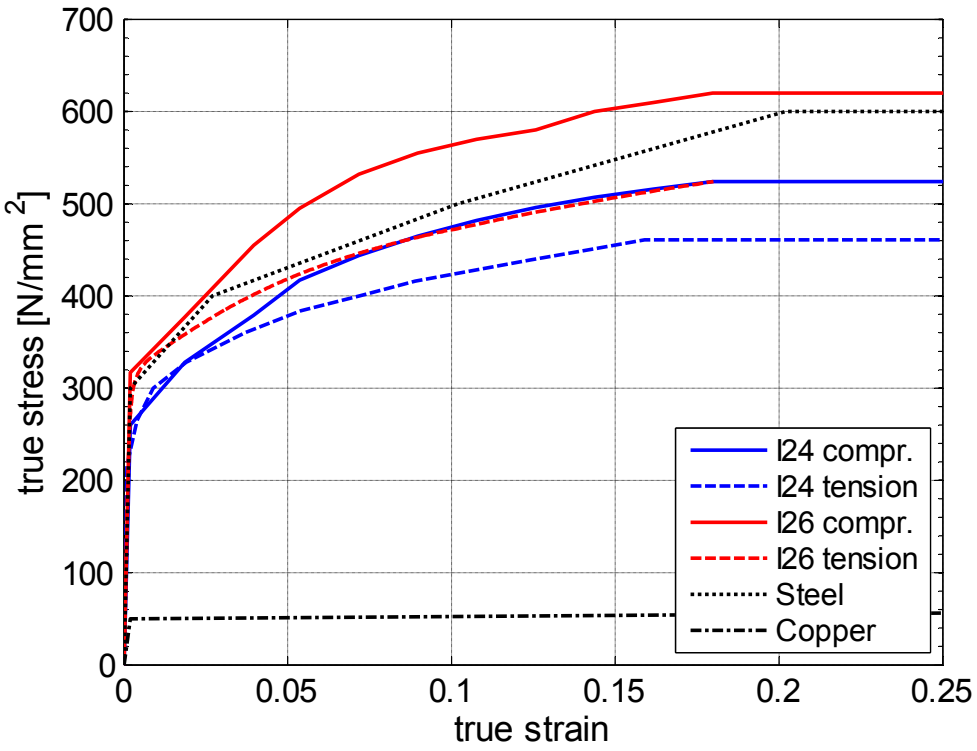

Figure 6: Stress strain curves for DCI insert I24 and I26, steel and copper.

3. Summary of the mock-up tests

3.1 Mock-up 1

Four load cycles were performed for Mock-up 1 with p_{max} = 40, 70, 100 and 130 MPa respectively. The residual radial deformation was measured manually after each load cycle as showed in Figure 7. Table 1 summarizes all the cycles with the main observations [7],[8].

Figure 7: Manual measurement of residual deformation fo Mock-up 1 after p_{max} = 130 MPa

Table 1: Summary of load cycles and main observations for Mock-up 1

Pressure Cycle	**p_{max} [MPa]**	**Time (ramp + hold) [sec]**	**Observation**
1	40	120+120	Copper tube deformed plastically corresponding to closure of 2 mm gap between insert and tube
2	70	320+120	As in pressure cycle 1
3	100	530+120	Onset of plastic deformation of insert. Residual radial deformation up to 5 mm
4	132	500+120	Large plastic deformations with residual radial deformation up to 20 mm. CIP pumping fluid into press during hold time indicating time dependent deformation.

In the final load cycle, for which the pressure was 132 MPa, the maximum residual radial deflection, Figure 8a, was measured to 20 mm and occurred at the location where the wall has its minimum thickness. The overall deformation was quite unsymmetric. The steel cassettes have partly debonded from the insert as shown in Figure 8b. The mock-up itself was however still “intact”, i.e. leak tight. Mock-up 1 was not loaded beyond 132 MPa to allow microstructural analysis of crack growth.

a) *b)*

Figure 8: a) Residual radial deflection at 130 MPa for Mock-up 1 b) debonding of steel cassette

3.2 Mock-up 2

The compression test for Mock-up 2 followed the same procedure as for Mock-up 1. Table 2 summarizes the load cycles and the main observations. Up to a pressure of 130 MPa the observations were similar to those of Mock-up 1. Main differences compared to Mock-ip 1 were that a deformation was registered at low loads and that the overall deformation was more symmetric than for Mock-up 1. At the end of the test load was increased until failure (139 MPa). As shown in Figure 9 the final collapse mode of Mock-up 2 was quite unsymmetric with a maximum indentation of 200 mm. A detailed post-test microstructural analysis of Mock-up 2 has not been done but from a visual inspection it was clear that cracks had propaged through the webs in this area. Thus the local failure was probably caused by initial defects that propagated at the failure load.

Table 2: Summary of load cycles and main observations for Mock-up 2

Pressure Cycle	**p_{max} [MPa]**	**Time (ramp + hold) [sec]**	**Observation**
1	40	50+120	Copper tube deformed plastically corresponding to closure of 2 mm gap between insert and tube
2	70	90+120	Some plastic deformation up to 3.5 mm
3	100	315+120	Onset of plastic deformation of insert. Residual radial deformation up to 4.5 mm
4	130	400+120	Large plastic deformations with residual radial deformation varying from 11.5 mm to 40 mm around mock-up perimeter.
5	139	855	Collapse of mock-up with pressure drop. A very large residual radial deformation of 195 mm at 90° marking.

Figure 9: Mock-up 2 after the pressure test

4. Finite element models of the Mock-ups

4.1 The Finite Element solver

The general finite element code ABAQUS was used for the finite element analyses in this report. ABAQUS has an implicit as well as an explicit formulation. The complete stiffness matrix is recalculated for each load step in the implicit formulation. For a nonlinear case the stiffness is re-calculated in each time step and each iteration until equlibrium is attained. There are no iterations in the explicit formulation due to lump formulation of the mass matrix. Thus the mass matrix is inverted with ease (matrix is diagonal). Otherwise that would be very time consuming.The numerical stability of the results requires that the time steps are below a specific value, $\Delta t \approx L_{\min} / c_d$, where $L_{\min}$ is the smallest element size and c_d is the dilatational wave speed. Thus the explicit formulation requires smaller time steps than the implicit formulation but each time step requires considerably less computational time. For highly non-linear (nonlinear material and large deformation) problems the explicit version is usually much faster than the implicit version. In fact is is often very difficult to get converged solutions with the implicit formulation (for more information on both formulations see [10]). The explicit formulation has therefore been adopted in the analyses below.

4.2 Finite Element meshes

A PYTHON script was written to allow automatic modelling of the geometry for different meshes. PYTHON is a script language, which is supported by the pre- and postprocessor ABAQUS/CAE.

The basic geometry data of the mock-up such as tube diameter, outer diameter of insert, dimensions of steel cassettes; and geometry variations i.e. corner radius of steel cassettes and the channel offset and the mesh densities for the three parts (steel cassettes, insert, tube) are defined in an input file called *input.params.py*. A main script, *run.cask.py,* is run in ABAQUS/CAE. *Run.cask.py* calls two other scripts for the definition of parameters (*comp.param.py* and *mat.params.py*) and then calls the scripts *part.cassette.py*, *part.insert.py* and *part.tube.py* for the creation of geometry and mesh for the steel cassettes, insert and tube respectively. The flow diagram in Figure 10 illustrates the different steps in the setup of the FE model.

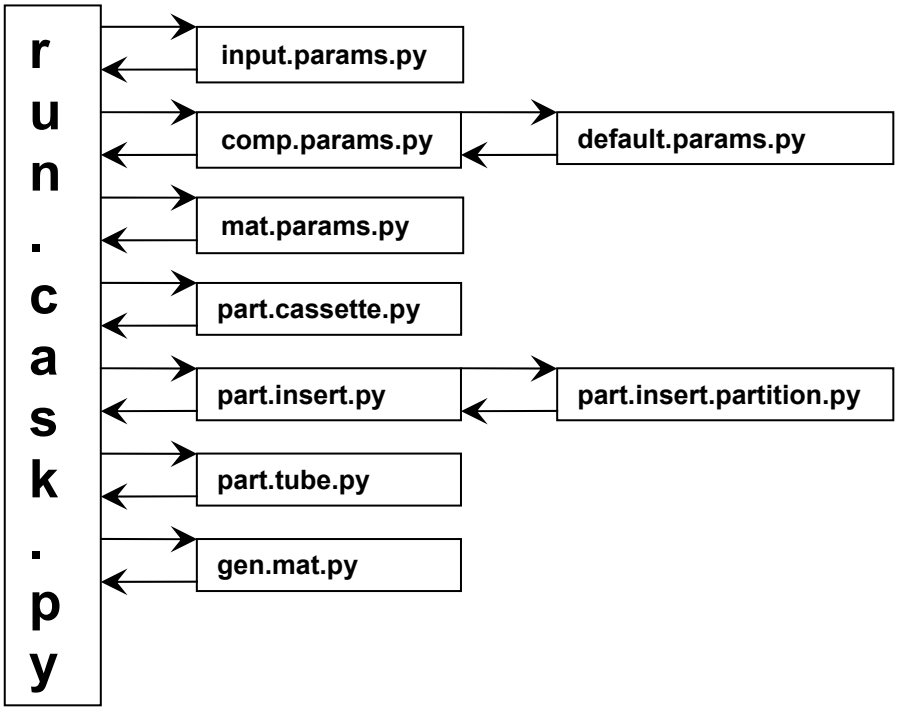

Figure 10: Scripts to build up the FE meshes

Scripts have the advantage that meshes are created automatically allowing a fast adjustment of design parameters and mesh densities. Figure 11 shows a 2D plane strain FE model with cassette corner radius 10 mm and no channel offset. This is the reference model for the design parameter studies.

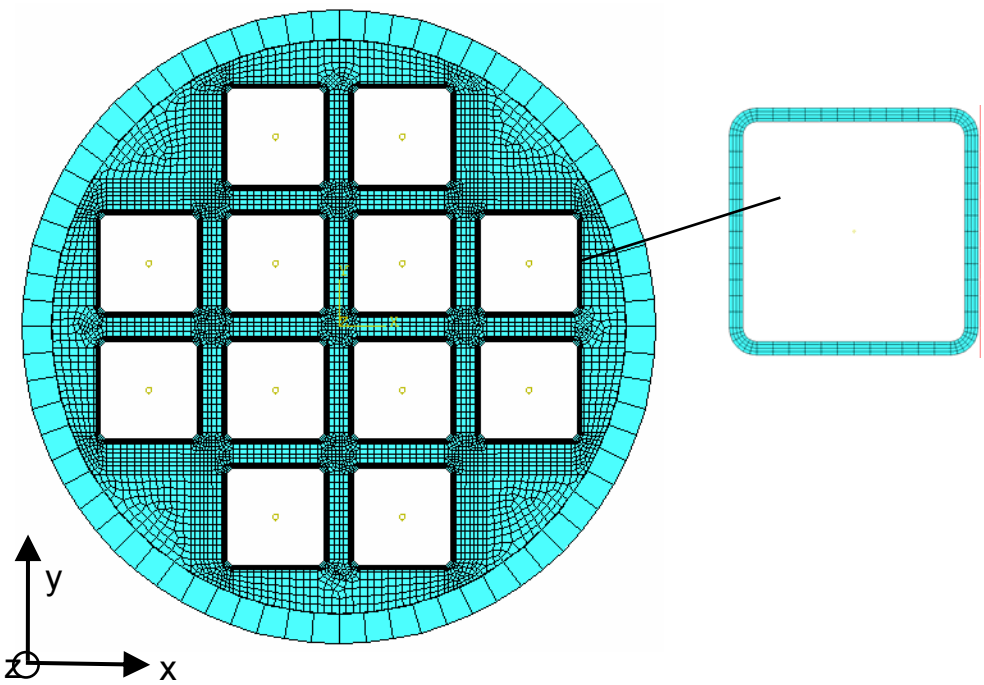

Figure 11: 2D plane strain FE model of the KBS-3 canister

The insert and the steel cassettes have a finer mesh than the copper tube. As Young's modulus and yield stress of copper is much lower than for DCI and steel, the mesh refinement of the copper tube has only a marginal effect on the results. Six different meshes, displayed in Figures 12a to 12f, were used to assess the mesh sensitivity. The coarse mesh (Figure 12a), the fine mesh (Figure 12c), the extra fine mesh (Figure 12d), the xx fine mesh (Figure 12e) and the xxx fine mesh (Figure 12f) had a uniform mesh refinement, i.e. each element was refined by the same factor. The locally refined mesh in Figure 12b had a selective refinement of elements.

The definition of load steps, constraints, loads and interactions between the different parts of the model was done manually with the pre-processor ABAQUS/CAE. It is important to note that symmetry planes should not be used to reduce the size of the FE-model in an instability problem. For instance the failure load could be severly underestimated if only a quarter of the geometry with associated symmetry conditions is modelled since non-symmetric failure modes can not be computed.

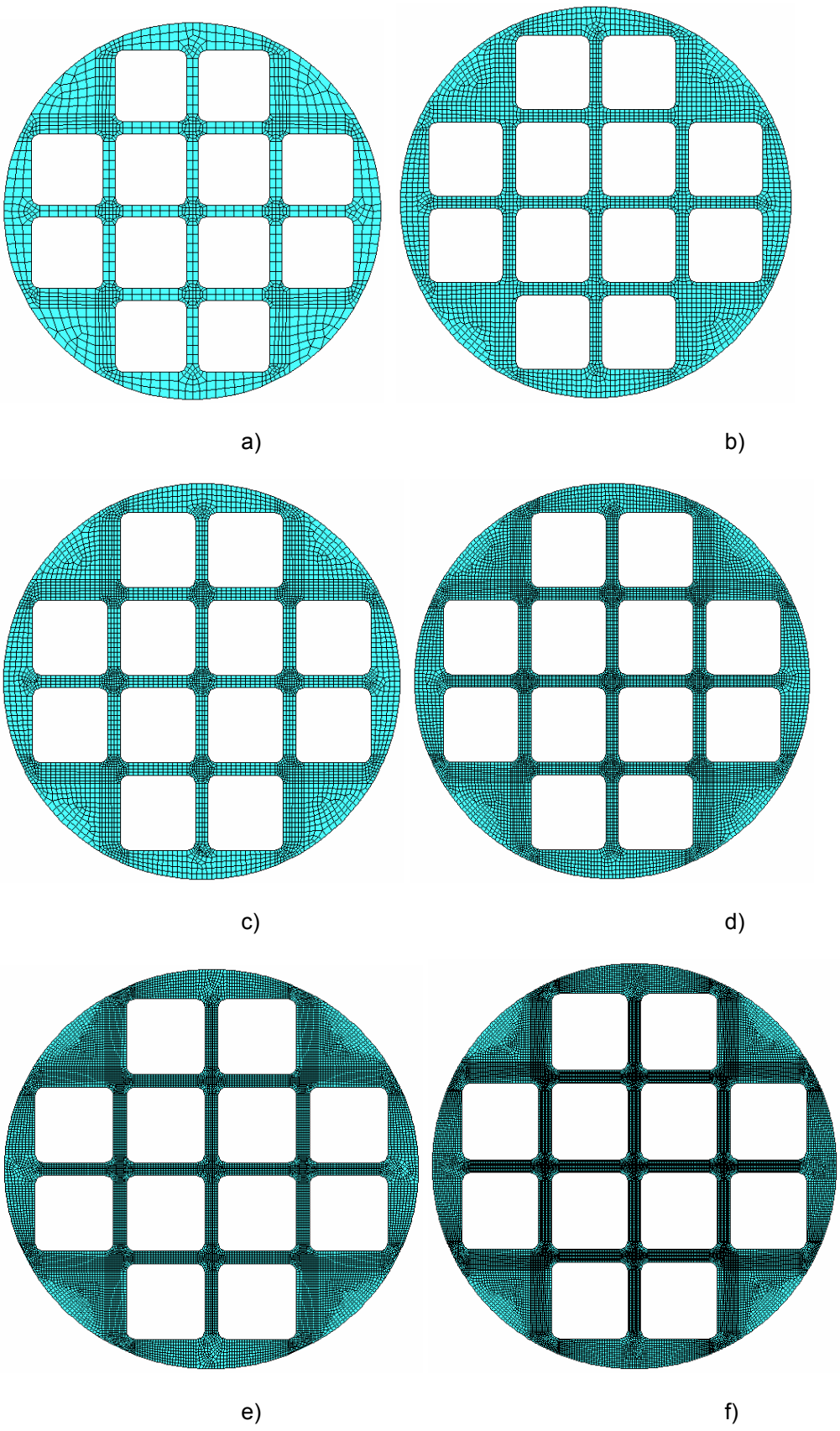

Figure 12: The five different mesh densities of insert with number of degrees of freedom for plane strain a) Coarse mesh (6704) b) locally refined mesh (14986) c) Fine mesh (18346, reference density) d) Extra fine mesh (28904) e) XX fine mesh (41848) f) XXX fine mesh (54542)

4.3 Boundary conditions and constraints

4.3.1 Boundary conditions and applied loads

To suppress rigid body motion of the two-dimensional model, the node in the centre has prescribed zero displacement and the top node of the insert has prescribed zero displacement in x direction (Figure 13). A pressure, p, is applied on the outer surface of the tube.

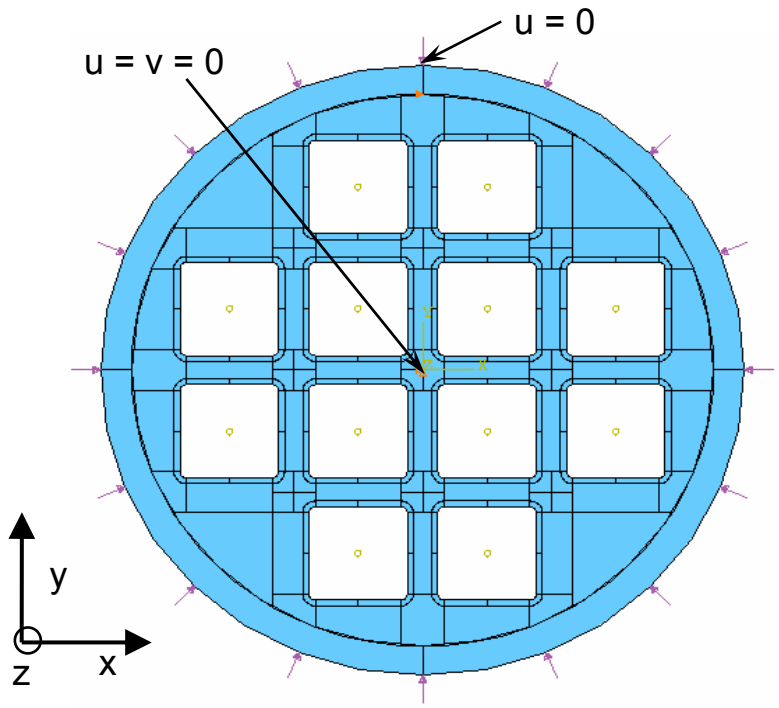

Figure 13: In-plane boundary conditions and load

4.3.2 Plane strain model (PS)

The two-dimensional plane strain model is the simplest one to simulate the plastic collapse and gives the shortest computational times. For plane strain[1] the displacement field is described by:

$$u = u(x, y), \quad v = v(x, y), \tag{1a}$$

which gives the following restraints of the z strain components,

$$\left.\begin{aligned} \varepsilon_z &= 0 \\ \varepsilon_{zx} &= \varepsilon_{yz} = 0 \end{aligned}\right\}. \tag{1b}$$

Due to the kinematic constraints the stress component in the z-direction will depend on the in-plane deformation. For an elastic isotropic material the relation is:

$$\sigma_{zz} = E \cdot \frac{\nu(\varepsilon_{xx} + \varepsilon_{yy})}{(1+\nu)(1-2\nu)}. \tag{1c}$$

It follows directly from Equation 1c that it is not possible to prescribe the axial stress component so that it balances the resultant force from the isoststic pressure in the z-direction.

[1] ε_z may also be constant but independent of the load. In the analyses below $\varepsilon_z = 0$

For plane strain FE models ABAQUS/Explicit the four-noded CPE4R element and the three-noded CPE3 element [7] were used here.

4.3.3 Generalized plane strain model (GPS)

A somewhat less restrictive assumption is to allow the in-plane displacements *u* and *v* to depend linearly on the axial component z and to allow that the axial strain depends on the applied load but is independent of the in-plane co-ordinates. This is referred to as *generalized plane strain*. The displacement field is then described by:

$$\left.\begin{aligned} u = u(x,y,0) + 2z\varepsilon_{xz}(x,y), \quad v = v(x,y,0) + 2z\varepsilon_{yz}(x,y) \\ w = z \cdot a(p) \end{aligned}\right\}. \qquad (2a)$$

The function *a(p)* depends on load, geometry and the material properties. This gives the following constraints for the strain components:

$$\left.\begin{aligned} \varepsilon_z = \varepsilon_z(p). \\ \varepsilon_{zx}(x,y) \neq 0 \,,\, \varepsilon_{yz}(x,y) \neq 0 \end{aligned}\right\}. \qquad (2b)$$

Hence the shear strains are functions of the in-plane co-ordinates. The value of these shear strains depend on the applied axial load. Figure 14 illustrates the basic difference between PS and GPS.

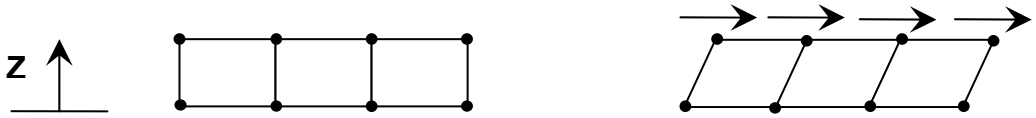

a) b)

Figure 14: Two-dimensional Illustration of difference between a) PS and b) GPS

Generalized plane strain may also be seen as “2.5 dimensional model” since the displacements depend linearly on z. The generalized plane strain FE model is implemeted by extruding the two dimensional FE mesh to a one-layer 3D mesh with linear elements and imposing the constraints. The w = w(z) condition is imposed by prescribing that all the nodes on the lower surface have zero axial displacement and that all nodes on the upper surface of the extruded model have the same axial displacement. The value of the axial displacement is a function of both the in-plane deformation and the axial load.

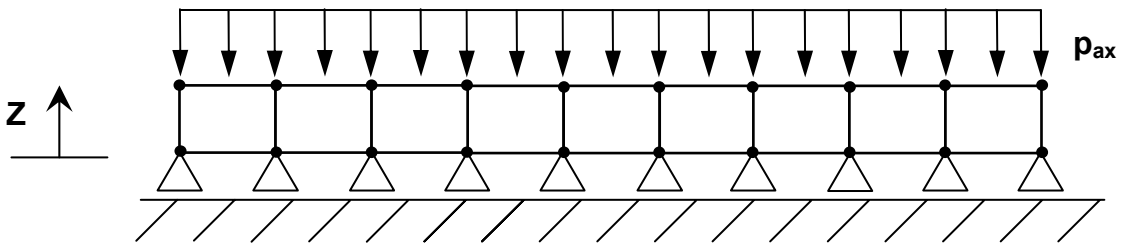

Figure 15: Loading and boundary conditions for the GPS model

The iso-static pressure gives a resultant load which is equal to $F_{ax} = A_{lid}\, p$, where A_{lid} is the area of the lid. In the FE analysis this load is evenly distributed over the insert cross-section area A_{ins} . The applied pressure in the FE analysis is therefore $p_{ax} = A_{lid} / A_{ins}\, p$. The insert radius is 474 mm and each fuel channels has an area of 160x160 mm^2. Thus the ratio $A_{lid} / A_{ins} = 1.77$

4.3.4 Three-dimensional model

The three dimensional (3D) FE model of the mock-up based on the mesh in Figure 12b is shown in Figure 16. In comparison to the 2D models the 3D model also contains the steel plates and the lids; thus the 3D model is a complete geometrical description of the mock-up.

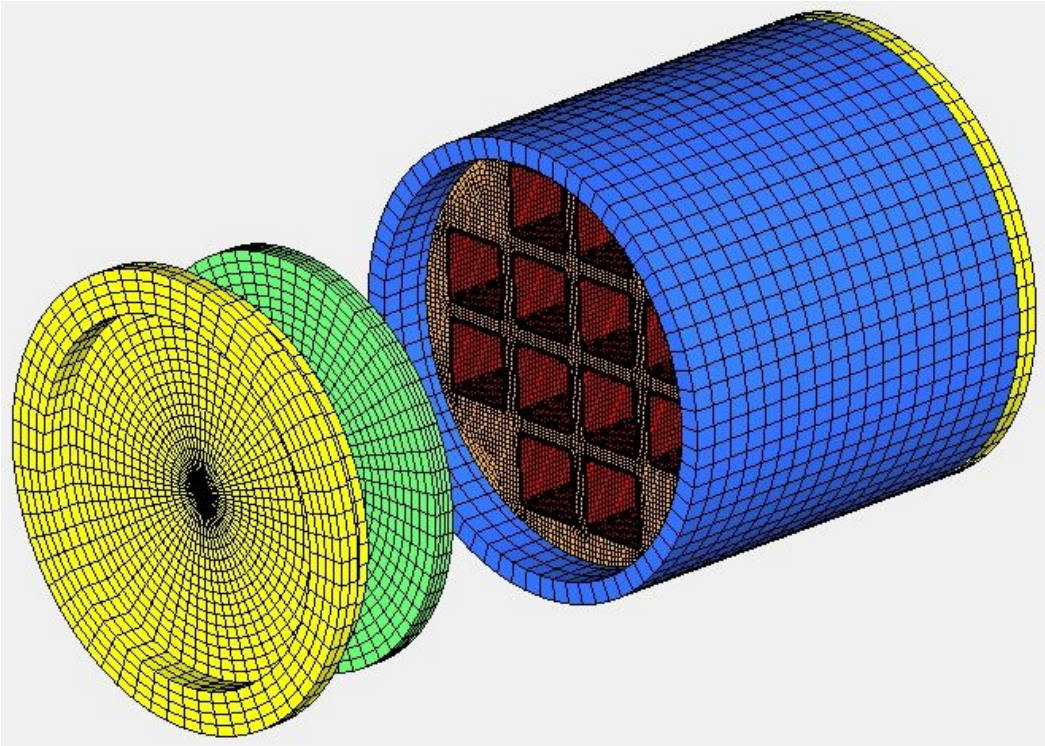

Figure 16: 3D model for Mock-up

The pressure *p* is applied on all outer surfaces of the 3D model of the Mock-up including the lids. The boundary conditions to suppress rigid body displacement are similar the ones for the GPS model with the exeption that they are applied to one of the lids and not to the insert.

4.4 Interaction between insert and cassette

The insert is cast around the steel cassettes. The cassettes should normally be strongly bonded to the insert but the bonding is not completely known. From the pressure tests of the mock-up canisters we know that some of the cassettes partly debond from the insert whereas others did not [7]. A lack of bonding will reduce the overall canister stiffness. A perfectly bonded cassette and a completely debonded cassette are modelled in the FE-analysis as follows:

- Complete debonding between cassette and insert is modelled as frictionless contact between insert and steel cassettes but where the cassettes also can separate from the insert.
- Perfect bonding between insert and cassette is modelled by having the steel cassettes fully tied to the insert.

The debonded case represents a displacement lower bound and the bonded case an upper bound of the real case. Figure 17 shows both interaction modelling approaches. For the interaction between the copper tube and the insert frictionless contact is assumed.

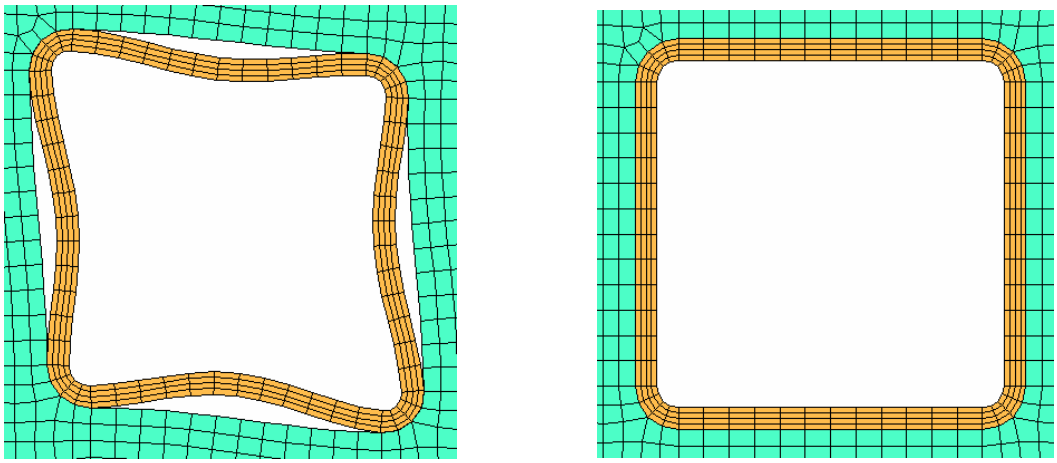

a) b)

Figure 17: a) Debonded cassette with partial contact separation and b) bonded cassette

In the 3D model frictionless contact is assumed for the interactions insert—steel plates, steel plates—lids and steel plates—tube. The lids are tied to the copper tube to avoid rotations of the whole structure.

4.5 Material properties

The Young's modulus, Poisson ratio and density for the three materials involved are given in Table 3. Figure 6 shows the stress-strain curves used to model the elastic-plastic behaviour. The stress-strain curves for steel and copper were taken from literature, whereas the ones for the inserts are from tension/compression tests done at JRC-IE [9]. Cast iron has a different behaviour in tension and compression. It is not possible to use different stress-strain curves for tension and compression in ABAQUS/Explicit. Since the inserts are mainly in compression, the compression stress-strain curves were adopted for the cast iron inserts in all analyses except one for which the tensile data was used. In the FE analysis the stress strain curve was defined directly by tabular values.

Table 3: Elastic material properties

Material	**DCI**	**Steel**	**Copper**
Young's Modulus [N/mm2]	170,000	210,000	130,000
Poisson Ratio	0.284	0.3	0.34
Mass Density [kg/m3]	7065	7850	8950

5 Results

5.1 Parameter Analysis

The reference model for the parameter studies has the following characteristics:

- plane strain;
- fine mesh for the insert as displayed in Figure 12c;
- compression stress-strain curve for the DCI
- corner radius of the steel cassette is 20mm
- no channel offset;
- debonded cassette;
- stress-strain curve from insert I24.

Table 4 lists the FE models that have been used for the parameteric studies.

Table 4: Overview of FE models for parametric studies

Main characteristic	PS/GPS or 3D	Mesh insert	Corner radius cassette [mm]	Channel offset [mm]	Interaction insert - cassettes	Stress-strain data for DCI
Reference	**PS**	**fine**	**20**	**0**	**Debonded**	**Comp.**
Coarse mesh	PS	coarse	20	0	Debonded	Comp.
Locally refined mesh	PS	loc. ref.	20	0	Debonded	Comp.
Extra fine mesh	PS	Extra fine	20	0	Debonded	Comp.
XX fine mesh	PS	XX fine	20	0	Debonded	Comp.
XXX fine mesh	PS	XXX fine	20	0	Debonded	Comp.
GPS	GPS	fine	20	0	Debonded	Comp.
3D	3D	loc. ref.	20	0	Debonded	Comp.
R = 10	PS	fine	10	0	Debonded	Comp.
R = 15	PS	fine	15	0	Debonded	Comp.
R = 25	PS	fine	25	0	Debonded	Comp.
Offset = 2	PS	fine	20	2	Debonded	Comp.
Offset = 6	PS	fine	20	6	Debonded	Comp.
Offset = 12	PS	fine	20	12	Debonded	Comp.
Partly debonded cassette	PS	fine	20	0	partly debonded	Comp.
Bonded cassette	PS	fine	20	0	Bonded	Comp.
DCI tensile stress-strain data	PS	fine	20	0	Debonded	Tension

Figure 18 shows the computed maximum radial displacement along, $\delta = \sqrt{u^2 + v^2}$, the outer surface of the insert versus the pressure for the reference model. Different deformed meshes are also shown for three loads. Figure 19 shows the deformed meshes with the associated von Mises iso-stress contours at p = 50, 120 and 124.3 MPa. Up to a pressure of 85 MPa the deformation is essentially elastic. At 85 MPa the deformation increases due to incipient yielding. The webs between the fuel channels start to bend and the steel cassettes start to debond from the insert. With further rising pressure all the webs between the fuel channels are bent and all the cassettes are more or less separated from the insert. At approximately 125 MPa the model collapses completely in a shearing dominated mode. The collapsed structure is completely compressed together and the fuel rod channels are virtually closed.

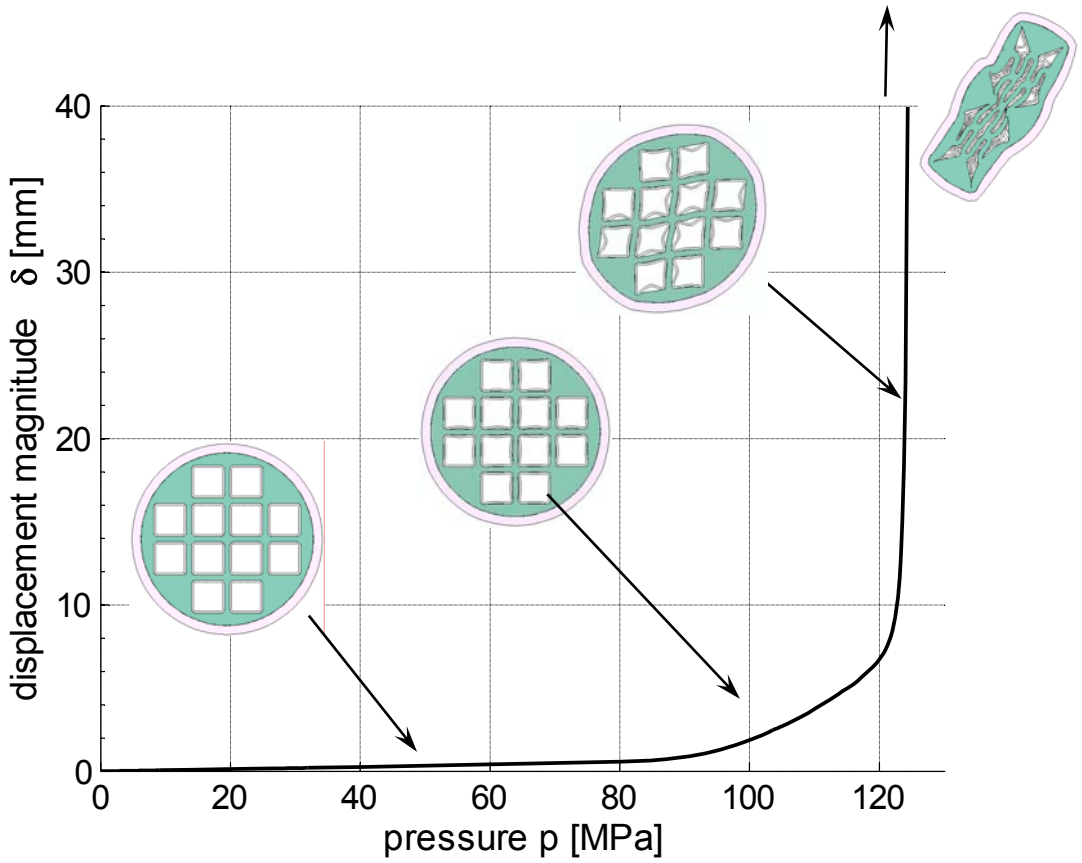

Figure 18: Computed maximum radial displacement along outer surface vs. pressure for the reference model

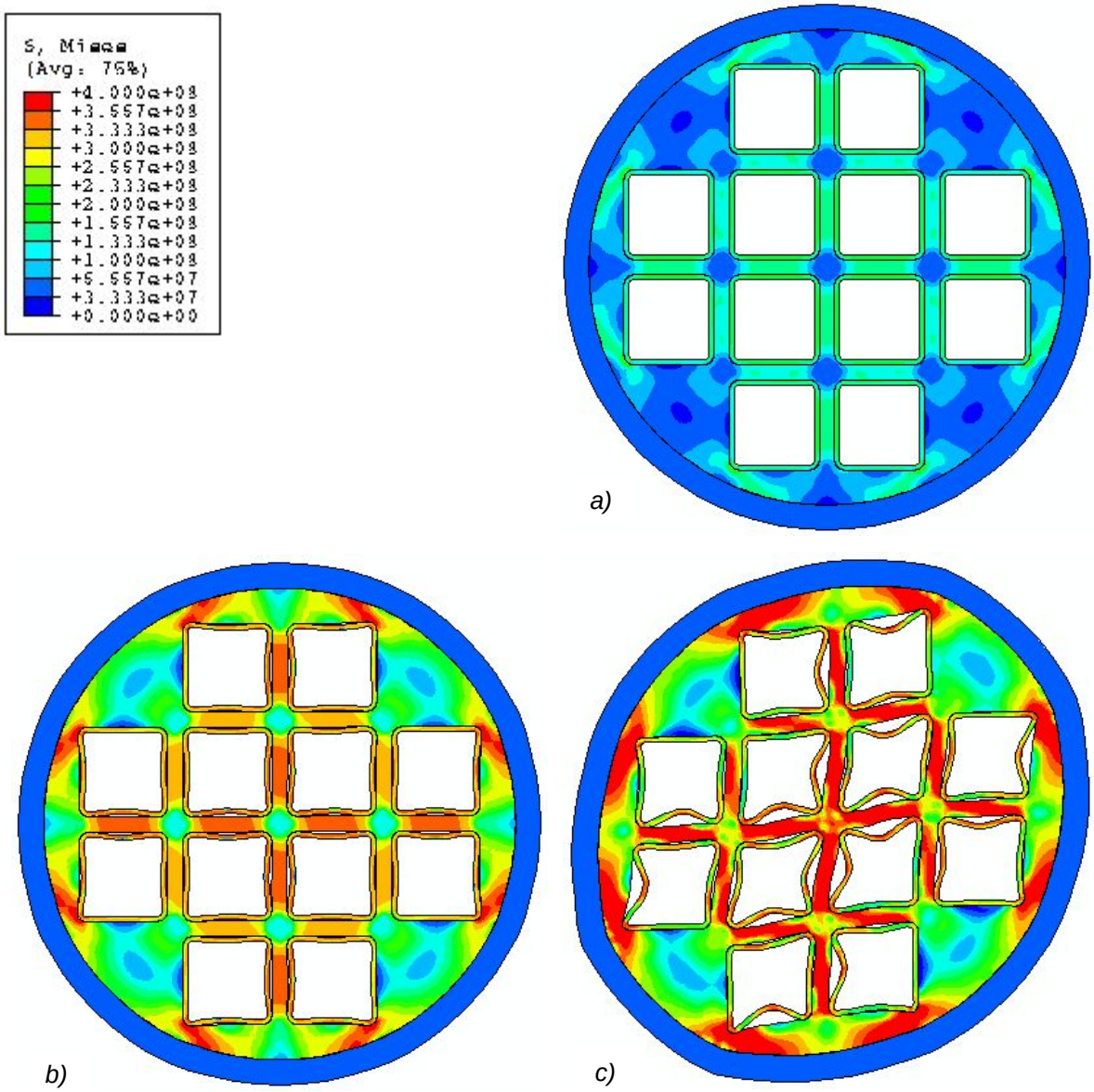

Figure 19: Deformed mesh with von Mises stress isocontours at p = (a) 50, (b) 120 and (c) 124.3 MPa

5.1.1 Mesh dependency of results

Figure 20 shows the computed maximum radial displacement along the the insert's outer surface versus the pressure for the different insert meshes in Figures 12a to 12f. There is clearly a strong mesh dependency. The collapse load decreases with increasing mesh density and appears to have converged for the two finest meshes. The convergence is better seen in Figure 21 where the pressure required for inducing maximum radial deflection of 5 and 15 mm is plotted versus the number of degrees of freedom. The trend for the uniform mesh refinement is monotonic. It may also be noted that the mesh with locally refined mesh is closer to the converged state than for the mesh with uniform mesh refinement. This indicates that the selective mesh refinement is more optimized.

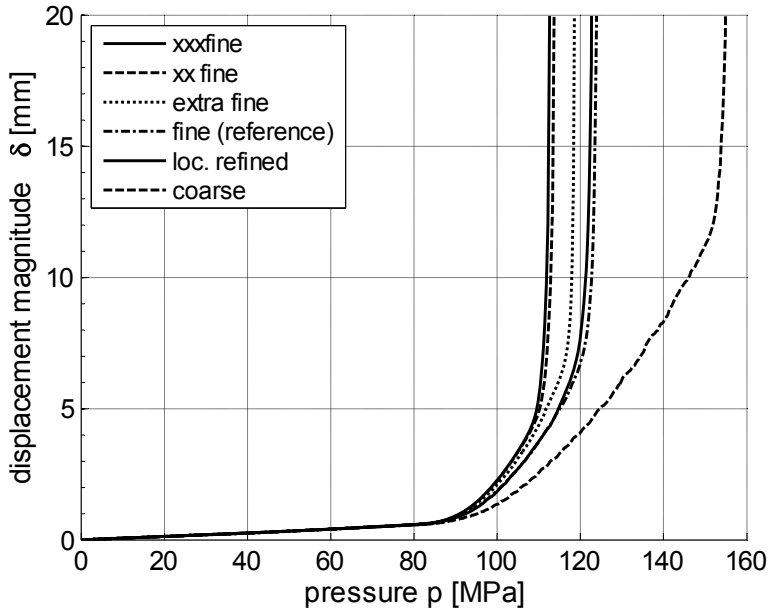

Figure 20: Displacement vs pressure for different mesh refinements

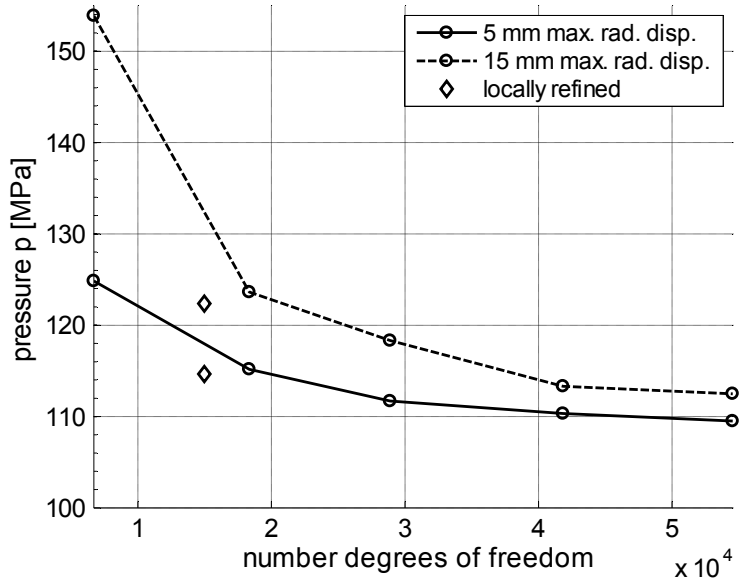

Figure 21: Applied pressure at maximum radial displacement 5 and 15 mm vs number of degrees of freedom.

Figures 22a to 22c show the von-Mises stress distribution at 110 MPa for different meshes. The finer the mesh the higher the overall level of the von Mises stress, especially around the outer corners of the outer cassettes.

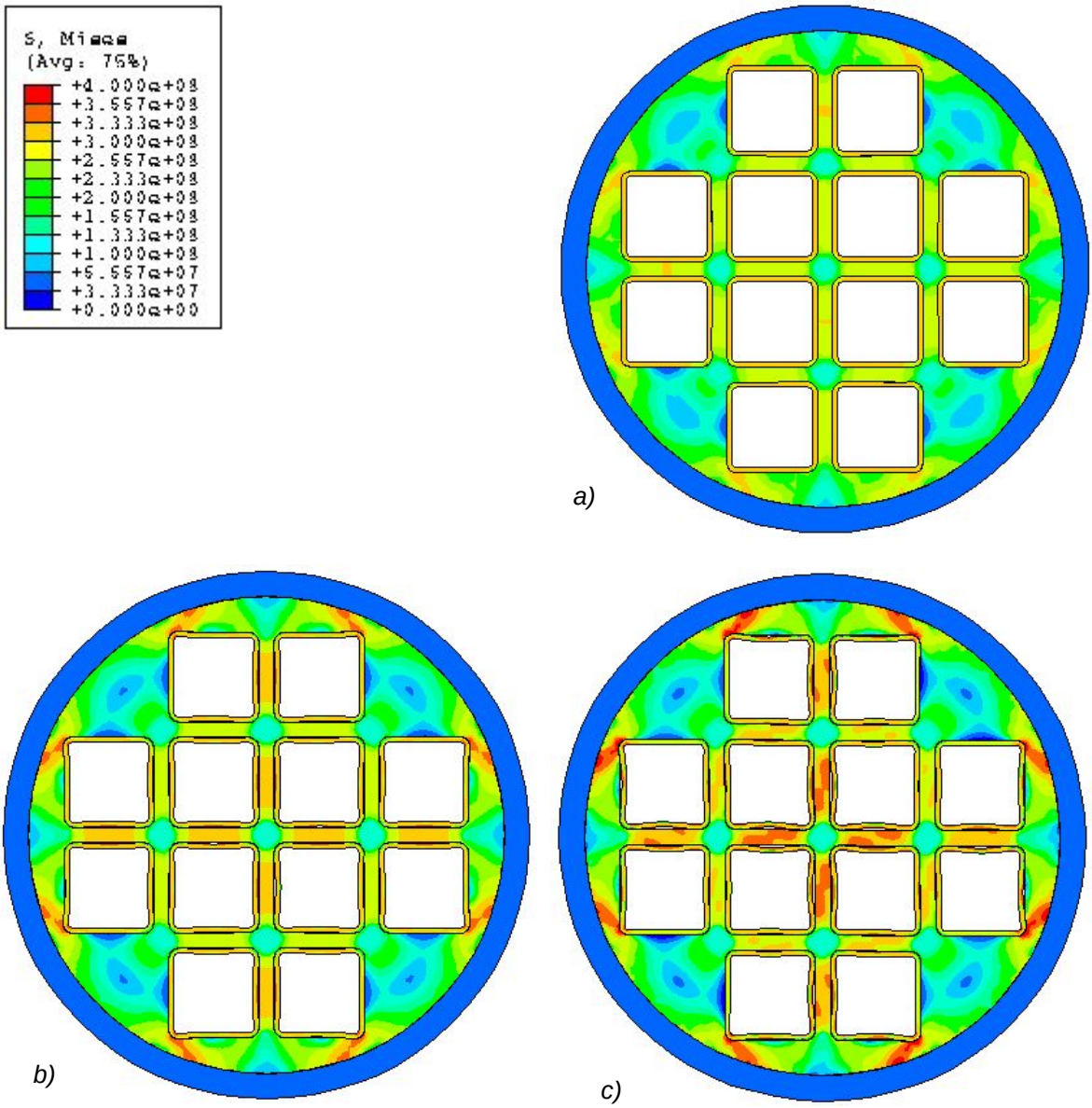

Figure 22: Deformed mesh with von Mises stress isocontours at p = 110 MPa for a) Coarse mesh b) Fine mesh c) XXX fine mesh

5.1.2 Geometric description of mock-up model

Figure 23 shows the computed maximum radial displacement along the insert surface versus the pressure for the plane strain, the generalized plane strain model and the 3D model respectively. The difference between the plane strain and the generalized plane strain model is very small and the plastic collapse loads only differ by a few MPa. The plastic collapse load of the 3D model, however, is much higher than for the plane strain and generalized plane strain models and loss of stiffness is less drastic. The displacements at a given pressure are lower and the shear mode, which occurred for the 2D models, does not occur in the 3D model. This can be seen from the von Mises stress isocontour plots at a maximum radial displacement of 14 mm in Figures 24a to 24c. The suppression of the shearing mode by the stiff lids and steel plate is the main reason for the overall increase in collapse load. Figures 25a to 25c show the von Mises stress isocontours for the three models at 110 MPa. The overall stress level before the plastic collapse is somewhat lower for the 3D model than for the plane strain and generalized plane strain model.

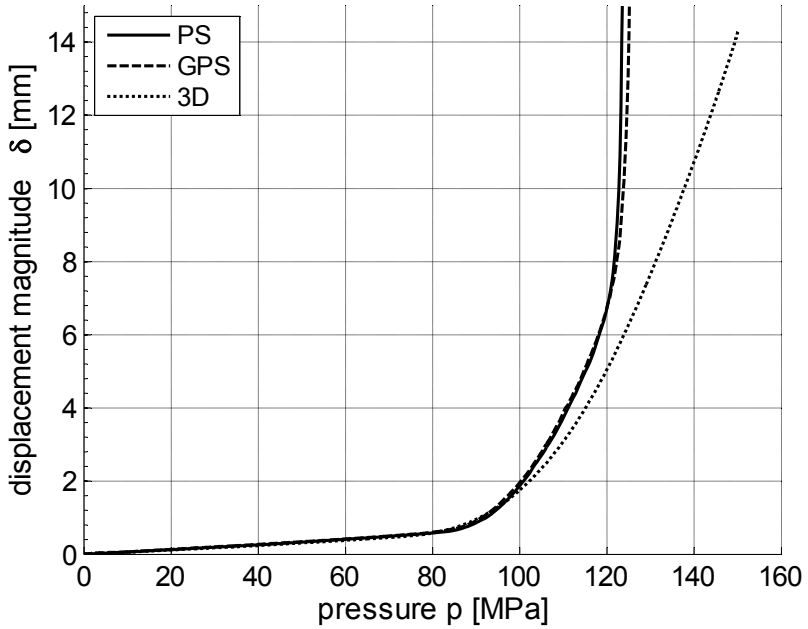

Figure 23: Displacement vs pressure for PS, GPS and 3D

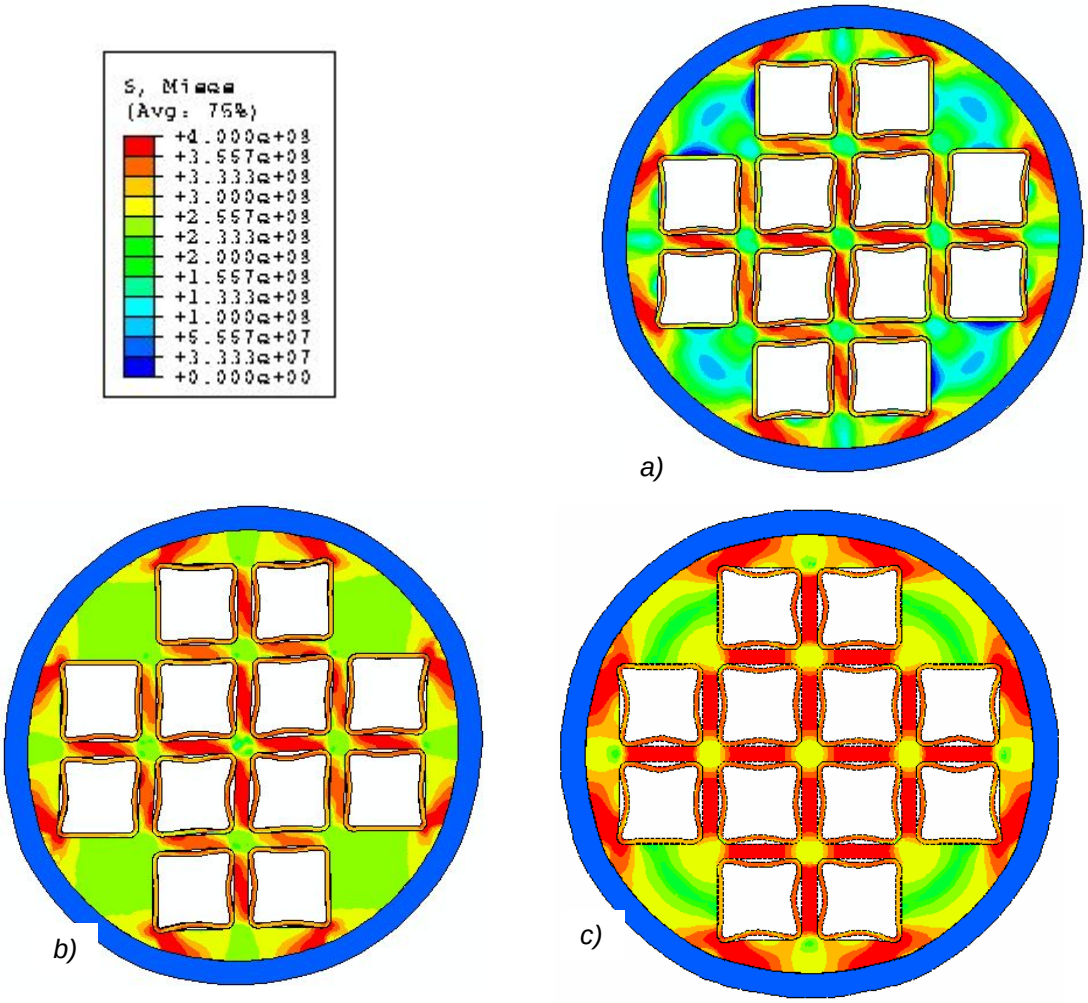

Figure 24: Deformed mesh with von Mises stress isocontours at max. radial displacement 14 mm for a) PS (123.4 MPa) b) GPS(125.3 MPa) c) 3D (149 MPa)

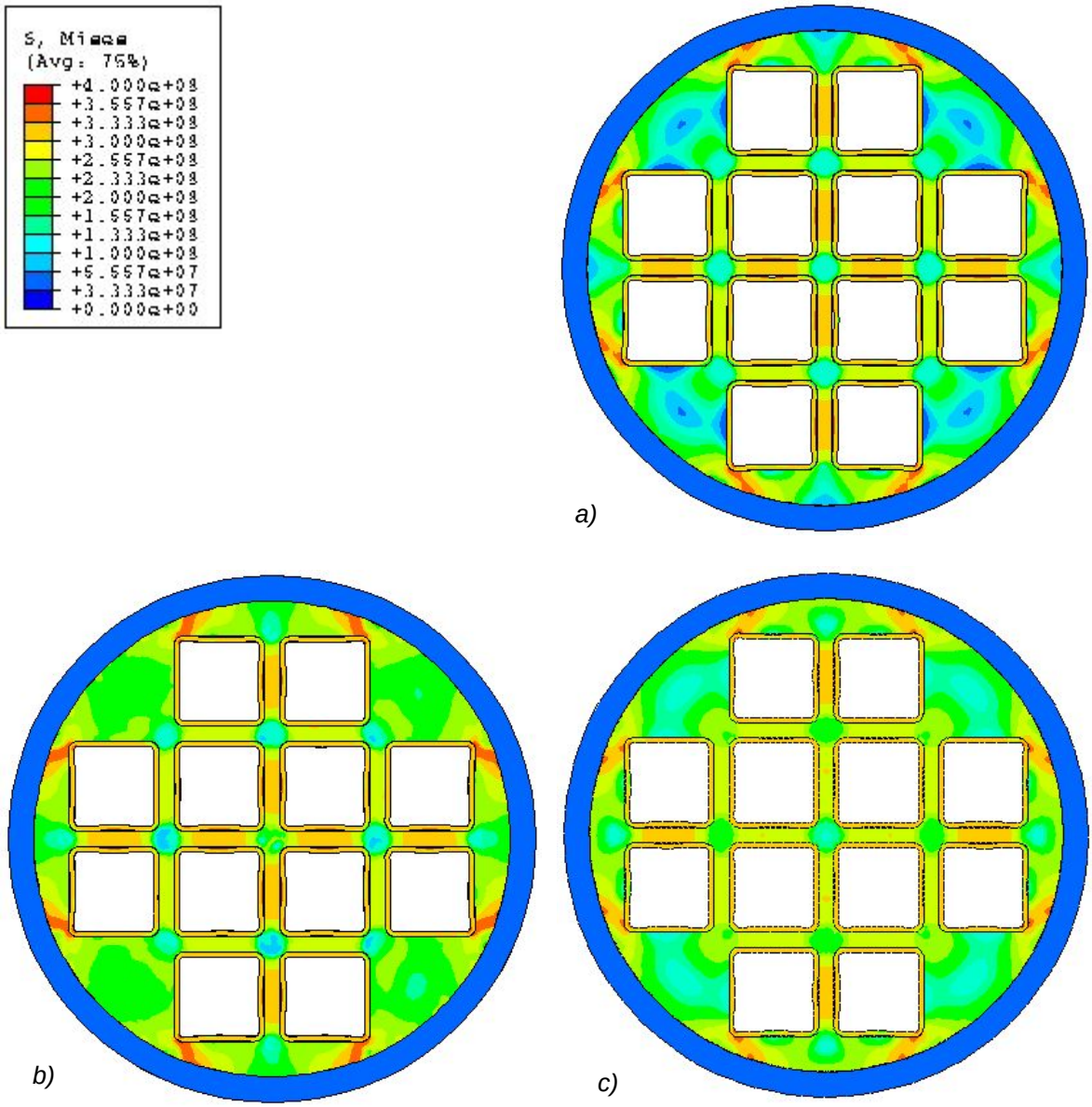

Figure 25: Deformed mesh with von Mises stress isocontours at p = 110 MPa for a) PS b) GPS c) 3D

5.1.3 Corner radius of the cassettes

Figure 26 shows the computed maximum radial displacement along the insert versus the pressure for different cassette radii. The most important observation is that variation in the corner radius only has a small effect on the collapse load. The second observation is that a smaller corner radius reduces the collapse load, which is expected due to its higher stress concentration factor.

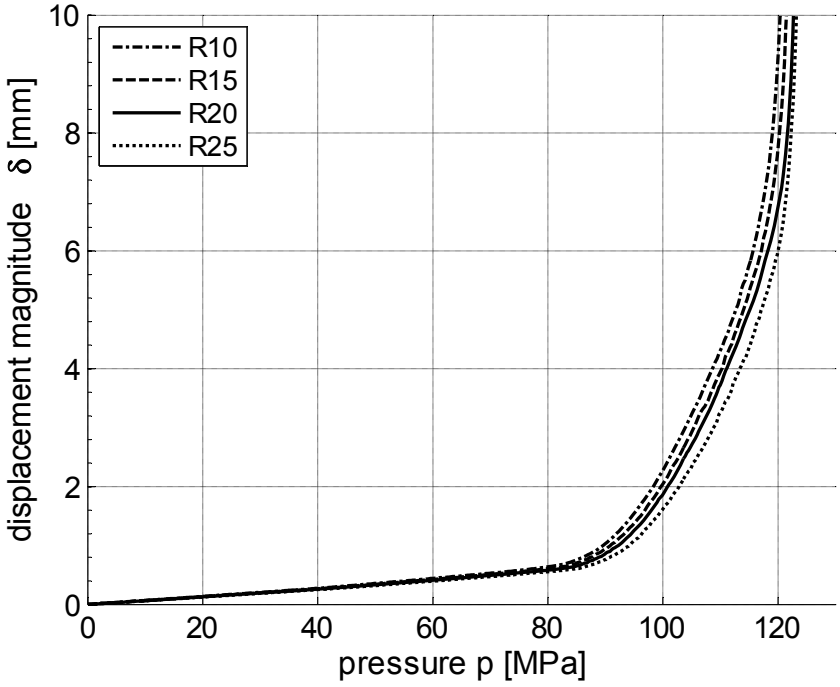

Figure 26: Displacement vs pressure for cassette corner radius 1, 15, 20 and 25 mm

5.1.4 Cassette offset

Figure 27 shows the computed maximum radial displacement along the outer surface of the insert versus the pressure for different fuel channel offsets and Figure 28 shows the applied pressure at 10 mm displacement versus the off-set. The maximum displacement increases and the plastic collapse load decreases gradually with increasing off-set. The 12 mm offset has quite a large impact on the collapse behaviour but for small values the effect is negligible. The channel offset has a larger impact than the corner radius of the steel cassettes for the values studied in this report.

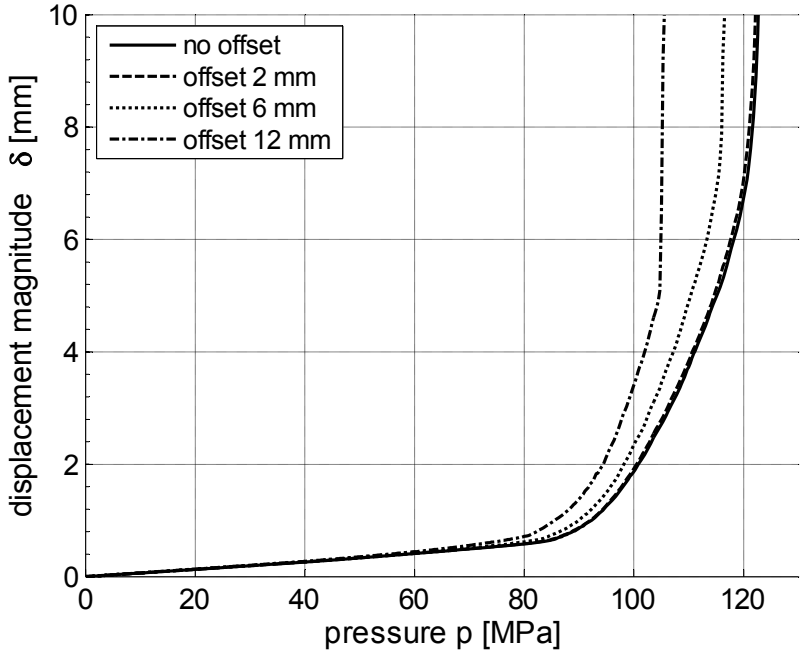

Figure 27: Displacement vs pressure for different offsets of the fuel rod channels

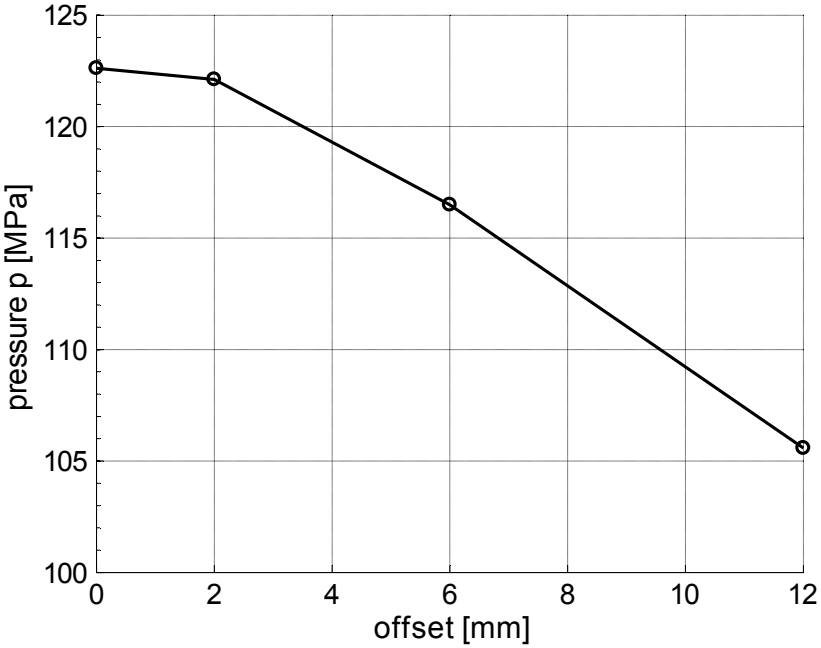

Figure 28: Applied pressure at maximal radial displacement of 10 mm versus offset

The offset changes the load distribution and the side with thinner wall will be more deformed and have higher stresses. The higher stress in the region with reduced wall thickness can clearly be seen from the von Mises stress isocontour plots in Figures 29a to 29c.

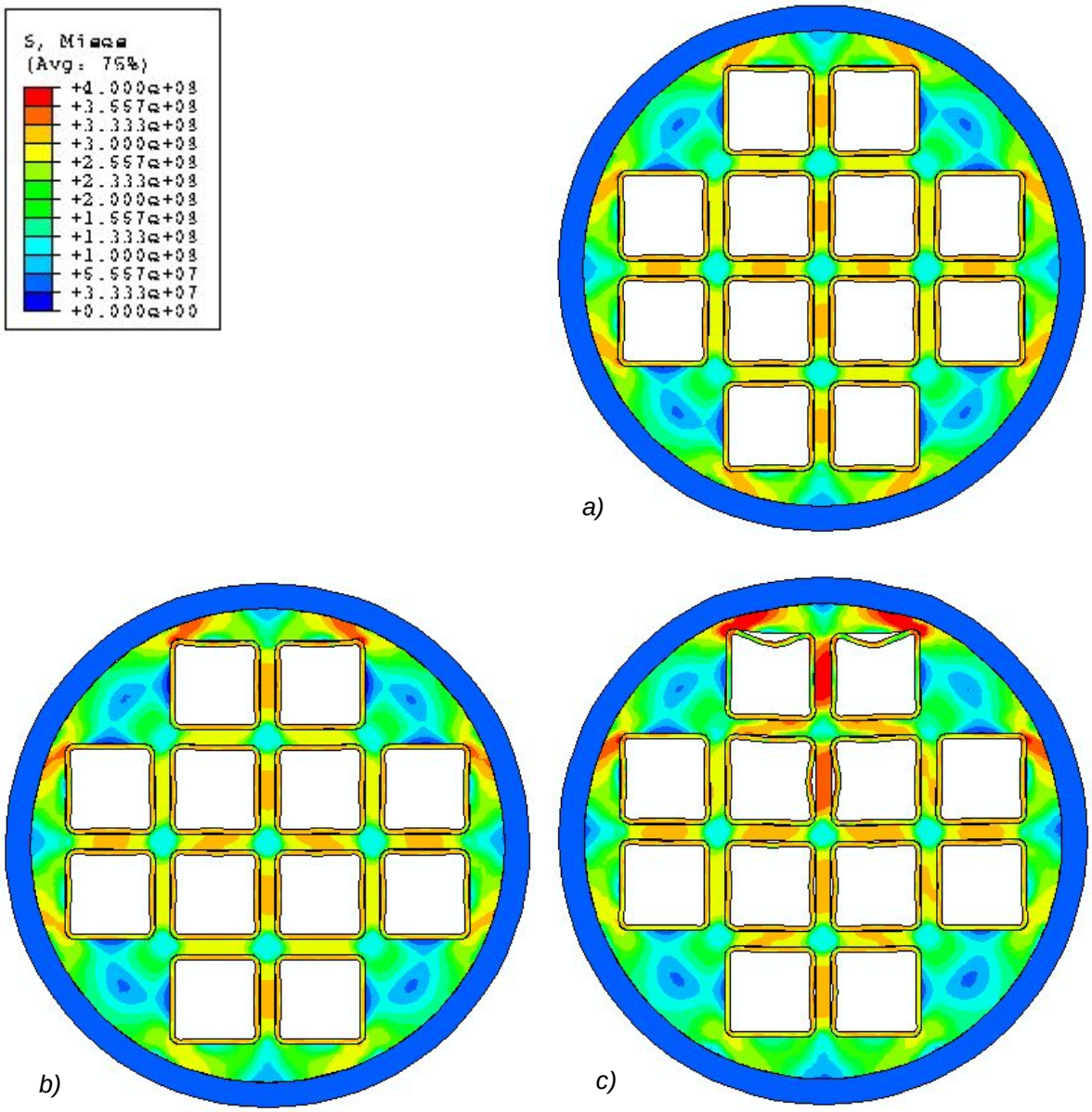

Figure 29: Deformed mesh with von Mises stress isocontours at p = 106 MPa for offset = 0 (a), 6 (b) and 12 (c) mm.

Figure 30 shows the deformation for the model with offset of 12 mm in slightly deformed and heavily deformed states. Due to symmetry loss it can be noted that the cassettes are not completely compressed as for the reference model with no offset.

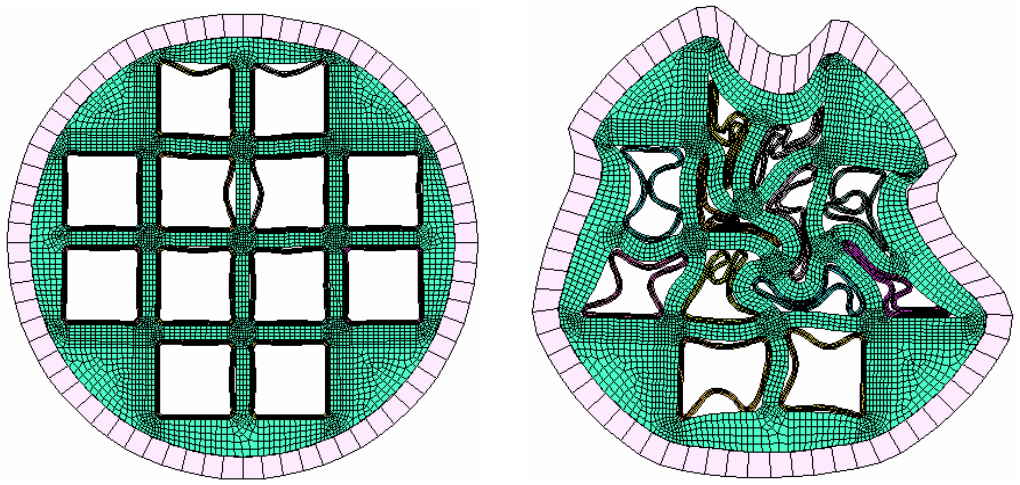

a) b)

Figure 30: PS model with offset 12 mm at a) p = 106 MPa and b) p = 112 MPa

5.1.5 Insert-cassette-interaction

Figure 31 shows the computed maximum radial displacement along the surface of the insert versus the pressure for the following three cases: i) all cassettes debonded, ii) all cassettes bonded; iii) two cassettes debonded the other ones bonded. As expected modelling the cassettes as bonded increases the overall stiffness resulting in a much higher plastic collapse load. It can also be seen in Figure 31 that the stiffness is significantly reduced when only the upper cassettes in Figure 10 are debonded. Figures 32a-c show the deformed mesh with von Mises isostress contours at 120 MPa for the three cases. Figure 32d shows the deformed mesh when the maximum radial displacement is 14 mm (p = 155 MPa) for the case where all the cassettes are tightly bonded to the insert. It is obvious that the bonded cassettes suppress the shearing mode observed for the debonded cassette case (Figure 24a). In fact the load-displacement curve is very similar to the 3D case with debonded cassettes (Figure 24c) and it can be concluded that the higher stiffness is caused by the suppression of the shearing mode. The stress concentration between the cassette channel and outer surface is not much affected, but the stresses in the internal webs are significantly increased by the debonding. As mentioned above it is very difficult to know to what extent the cassettes are bonded but the effect on plastic collapse is quite strong. This uncertainty with its associated variation in stiffness will clearly pose a problem for assessing a best-estimate prediction.

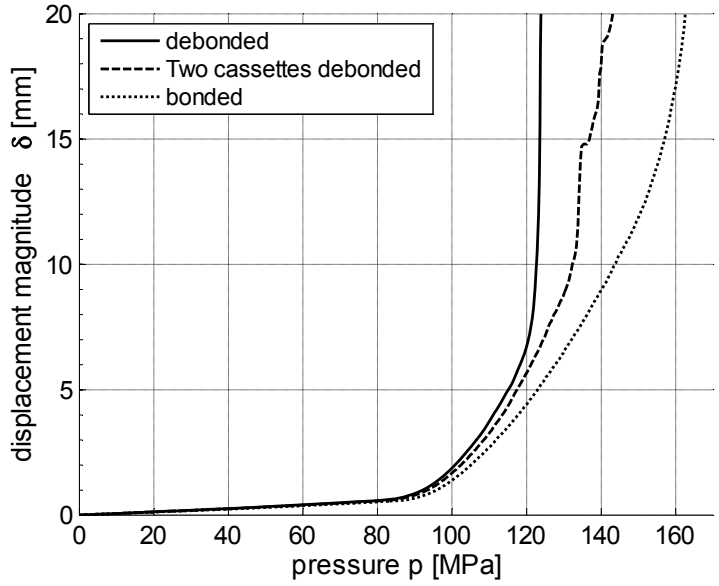

Figure 31: Displacement vs pressure for different insert-cassette interaction definitions

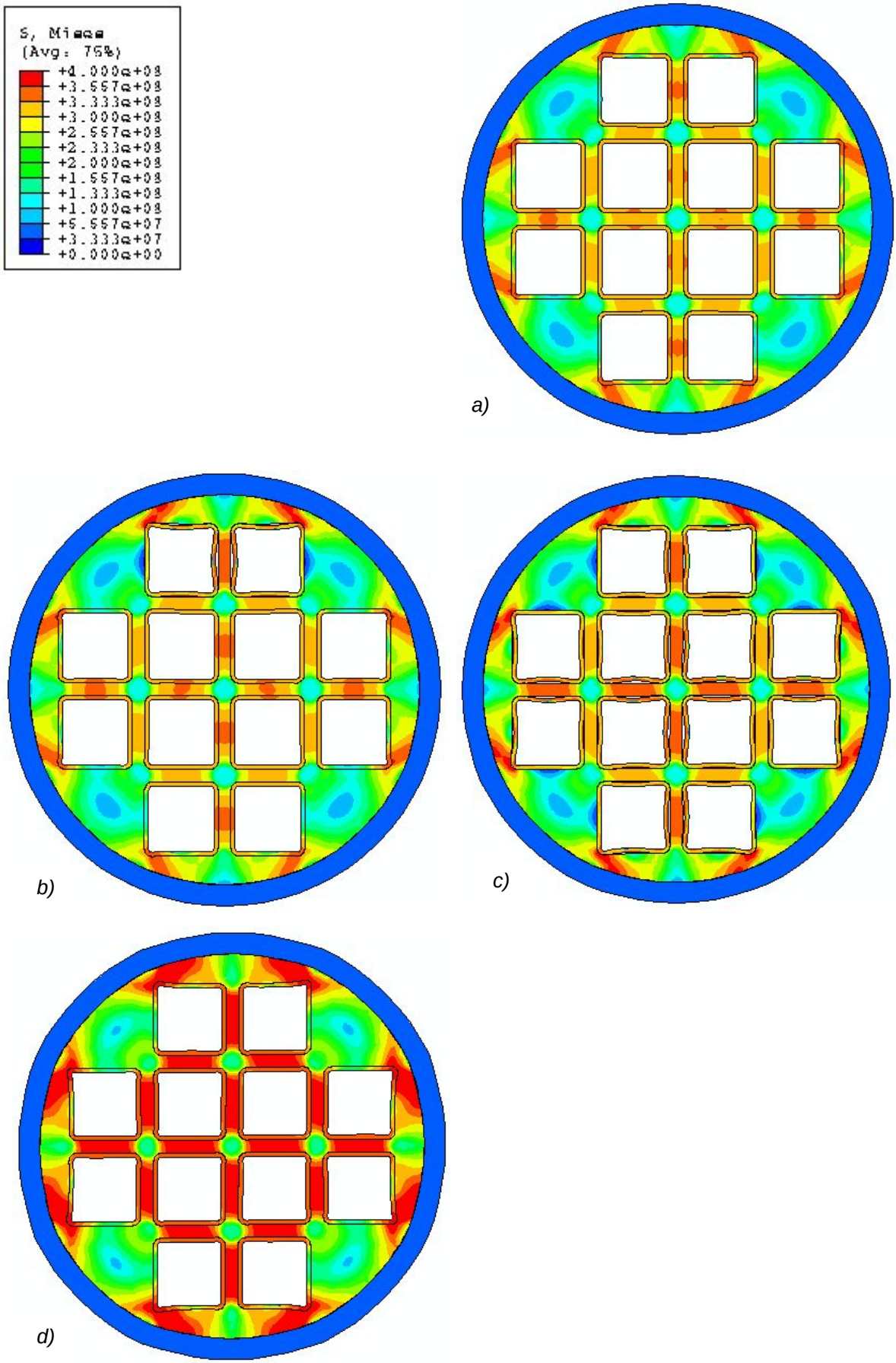

Figure 32: Deformed mesh with von Mises stress isocontours for a) Bonded cassettes p = 120 MPa b) two cassetted debonded p = 120 MPa c) all cassettes debonded p = 120 MPa d) radial displacement 14 mm for the case with all cassettes bonded p = 155 MPa.

5.1.6 Compression vs tensile DCI stress-strain curve

Ductile cast iron is much stiffer in compression than in tension as shown in Figure 6. At lower loads local tensile stresses develop at the highly stressed region between the cassette channel and the outer surface. When the load is further increased the region with tensile stress extend. Figure 33 shows the regions for which the first principle stress is larger than 0, (which is an indication of the tensile regions) at p = 95 and 120 MPa. Although only a small part of the total volume will be in tension it can still have a large impact impact on the collapse load. As mentioned above the explicit ABAQUS formulation does not allow a material model that is different in compression and tension. Analyses were therefore performed using the compression data. Figure 34 shows the maximum radial displacement versus the applied load using the compressive and tensile stress-strain data from insert I26 respectively. One would expect the relative difference in collapse load to match the difference in stress-strain curves but the computed difference is much smaller. Figure 35 depicts the associated deformation and the stress state at p = 120 MPa using compressive and tensile properties respectively.

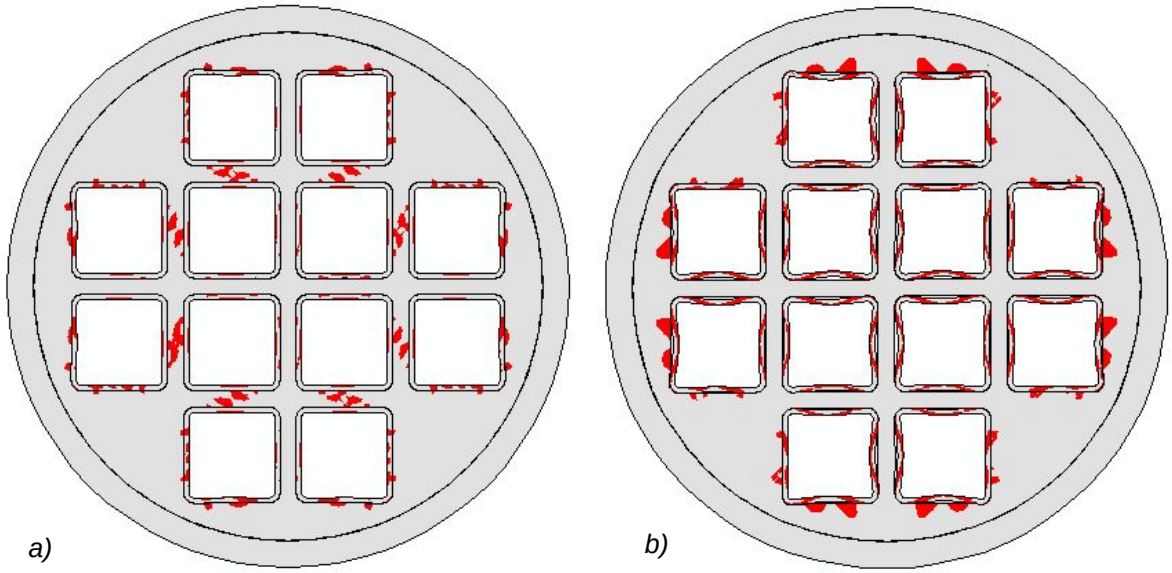

Figure 33: First principle stress for reference model at a) p = 95 MPa b) p = 120 MPa.

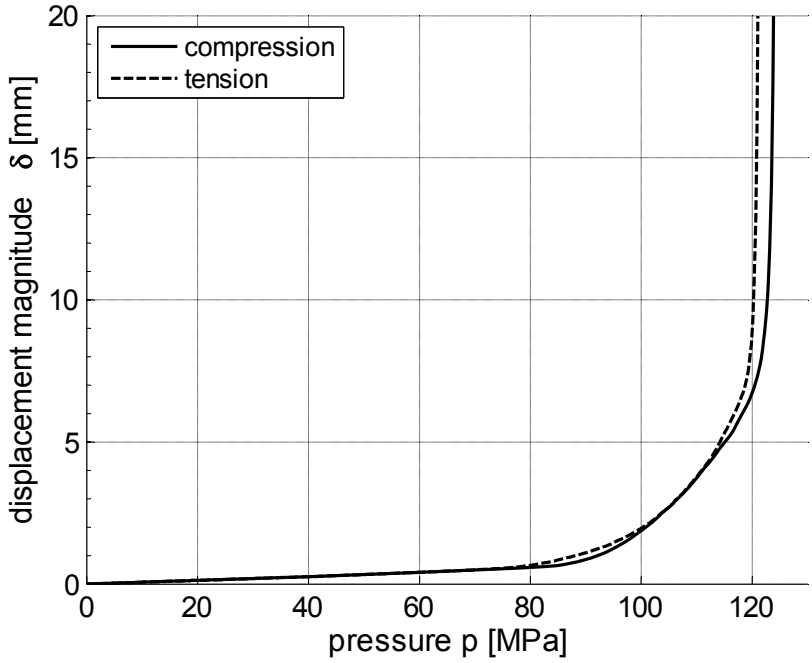

Figure 34: Displacement vs pressure with compressive and tensile stress-strain data for DCI.

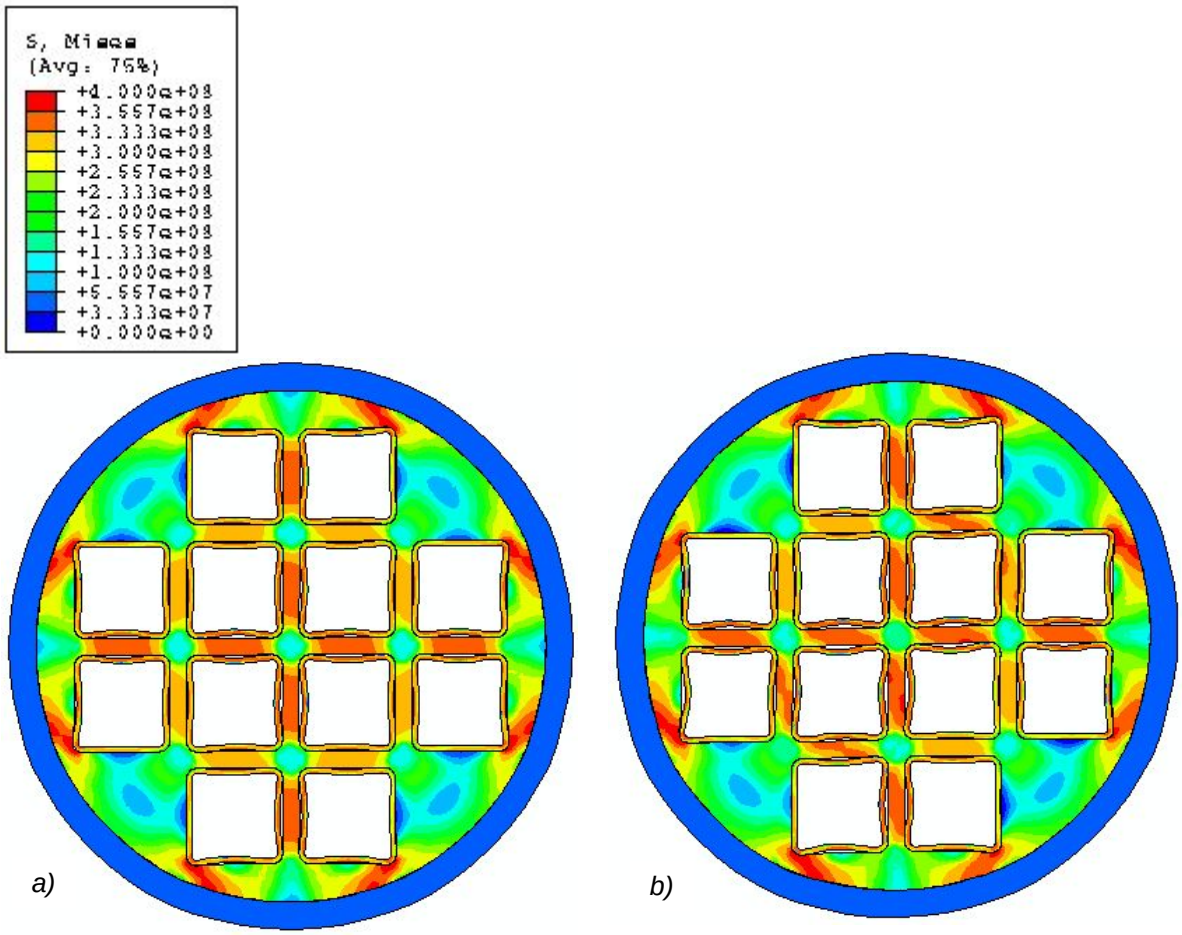

Figure 35: Deformed mesh with von Mises stress isocontours at 120 MPa for a) compressive DCI stress-strain data b) tensile DCI stress-strain data.

5.2 Comparison with mock-up tests

Table 5 summarizes the modelling characteristics used to model the two mock-up tests. Since the debonding is not known, models with the upper (bonded) as well as lower bounds (debonded) have been used. The mesh convergence investigation indicated that the xx fine mesh gives displacements that are very close to the converged state; the xx fine mesh was therefore used for all plane strain models. In the two-dimensional models the plastic collapse occurs in a mode dominated by shearing. This shearing is suppressed by the stiffening effect of the lid and steel plate which is only modelled by the 3D model. The computational times are very long for the 3D models and only results for the mesh corresponding to the locally refined mesh are therefore included. In Figure 20 and 21 the failure load for the 2D model was about 10% higher for the locally refined mesh than for the xx-fine mesh. One could therefore expect that the 3D model also gives a failure load which is 10% too high.

Table 5: Overview of FE models of mock-ups

Mock-up	Geometry	Insert	Mesh insert	Corner radius cassette [mm]	Channel offset [mm]	Interaction insert - cassettes
1	PS	I26	XX fine	20	12	debonded
1	PS	I26	XX fine	20	12	bonded
1	3D	I26	Loc. ref.	20	12	debonded
1	PS	I26	XX fine	20	12	Two cassettes debonded, the rest bonded
2	PS	I24	XX fine	10	0	debonded
2	PS	I24	XX fine	10	0	bonded
2	3D	I24	Loc. ref.	10	0	debonded

5.2.1 Mock-up 1

Figure 36a and 36b show the measured and computed radial displacement for Mock-Up 1 at the two locations with the largest and smallest measured deformation versus the applied pressure. These locations are indicated in the Figure insert. The computed displacements in Figure 36a are for the 2D model with all cassettes bonded or debonded and the 3D model with debonded cassettes and in Figure 36b) for the three 2D models. As described above, the reported measured values during the loading were measured manually from the outside of the copper tube after each load cycle. The inner diameter of the copper tube is nominally 2 mm larger than the insert radius. If the insert is centrally located then the gap between the insert and the tube should be 1 mm. But we don't know the exact position of the insert so it is also possible that the gap can vary between 0 and 2 mm along the insert's surface. Because of copper's very low yield stress and hardening, the gap will be closed already at 10 MPa pressure. The first measured value is at 45 MPa for which the residual deformation of the insert should be very small. Thus we assume that the measured deformation at 45 MPa is only by closing the gap. The measured data for the insert in Figure 36 are therefore the measured data from the copper tube with the measured value at 45 MPa subtracted. The measured displacement curves lie between the bonded and debonded curves with the two-dimensional model. The very sudden stiffness loss for the debonded plane strain model is due to the shearing mode failure. The 3D model with debonded cassettes and the plane strain model with all cassettes debonded have a similar behaviour but they are both stiffer than what the test data suggest. The collapse load for the 2D model with only two cassettes debonded is very close to the measured value. It can also be noted that the difference in displacement between the two locations is larger in the test than in all computational models.

Figure 37a and 37b show the measured deformation profile of the insert after the test and corresponding computed deformation profiles. These measurements were performed directly on the inserts after the copper tube had been removed by laser technique and hence more reliable than the values measured during the test. The maximum measured deformation was 18 mm. The computed curves have been taken from the load at which the displacement was as close as possible to 18 mm. All displacements in Figure 37 have been

normalized so that the maxiumum displacement in the plot is 80 mm. The model assumptions in Figure 37a and 37b are the same as in Figure 36a and 36b. The shearing mode, which is computed in the plane strain case with debonded cassettes, is not seen in the actual test. The local implosion at the location with the thinner wall in the measured data can be seen in the different calculations. The measured deformation in the lower part of the plot is only 10% of the value in the thin-walled part. In the calculations, however, the deformation in the lower part is more than 50% of the value in the thin-walled part for the 3D model and the 2D models with all cassettes either debonded or bonded. For Mock-up1 only the cassettes in the thin-walled part had debonded. Clearly the best fit with the experimental profile is attained for the case with two debonded cassettes. Thus it may be surmised that only the cassettes in the thin-walled region had debonded.

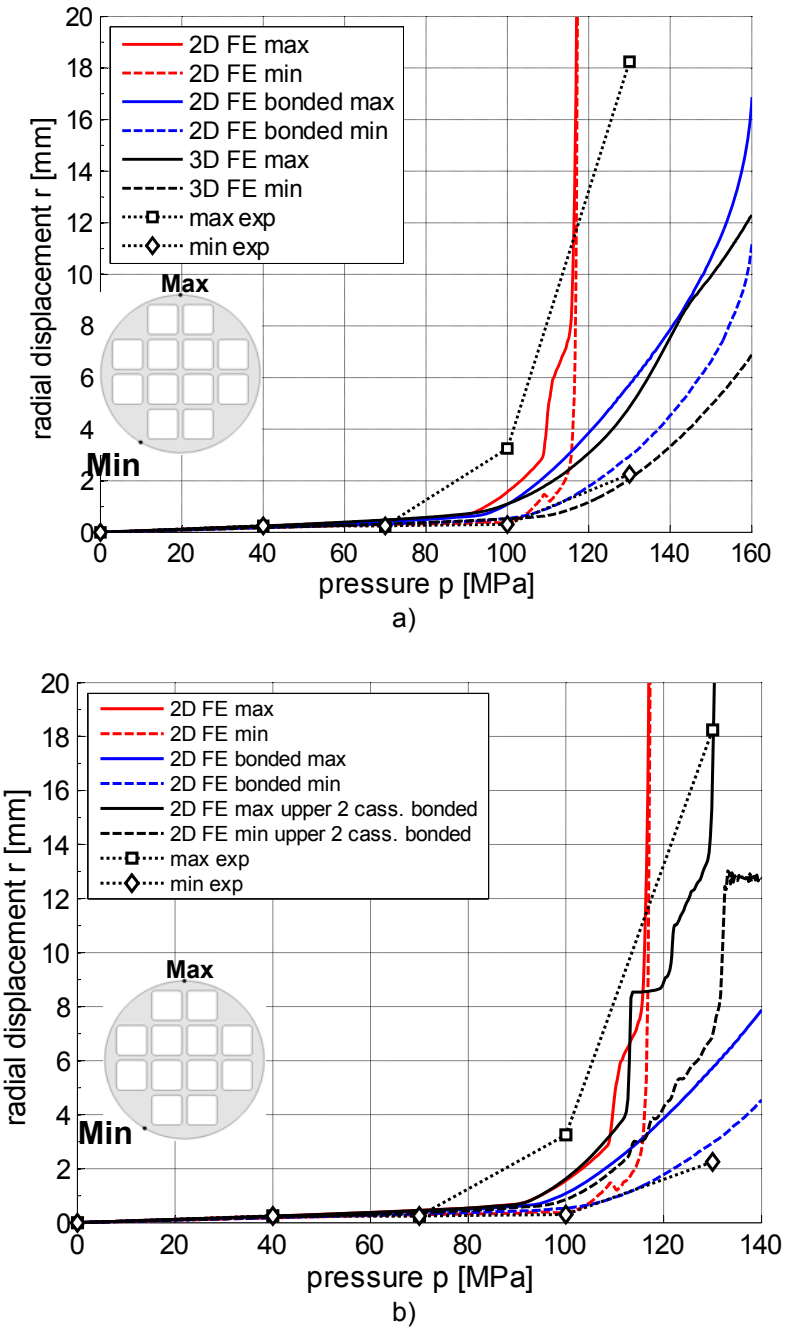

Figure 36: Displacement vs. pressure for Mock-up 1 computed and measured values with bonded and debonded cassettes together with positions of minimum and maximum radial displacement. Max and Min indicates the locations at which the displacements were evaluated a) measured value and computed 3D and 2D with debonded cassettes and 2D with bonded cassettes b) measures values and 2D plane strain model with all cassettes dobonded, all cassettes bonded and the two top cassettes debonded and the others bonded.

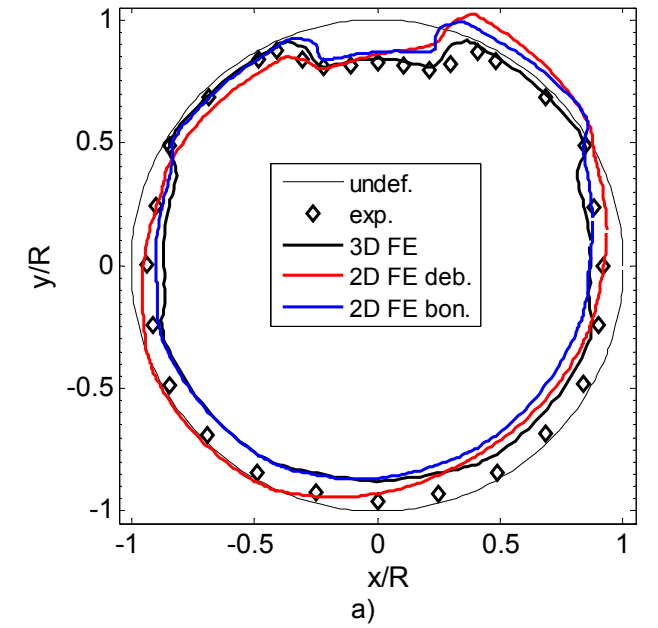

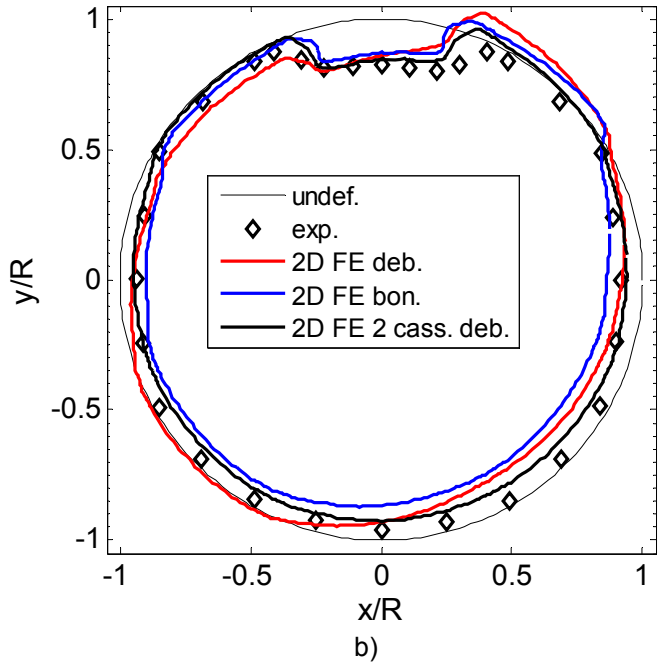

Figure 37 Measured and computed radial deformation when maximum deformation is 18 mm a) measured value and computed 3D and 2D with debonded cassettes and 2D with bonded cassettes b) measures values and 2D plane strain model with all cassettes dobonded, all cassettes bonded and the two top cassettes debonded and the others bonded.

5.2.2 Mock-up 2

Figure 38 shows the computed and experimental radial displacement of the insert versus the pressure for Mock-up 2 at the locations with maximum and minimum measured values. The collapse for the plane strain FE model with debonded cassettes occurs at approximately 108 MPa, which is significantly lower than the measured collapse load. The plane strain FE model with bonded cassettes collapses at about 160 MPa, which is higher than the measured value. The load displacement curve for the 3D model with debonded cassettes follows the 2D plane strain model fairly accurately up to 150 MPa. The measured load-displacement curve follows the 3D model and 2D model with bonded cassettes reasonably up to the failure load. The plastic collapse in the test was quite drastic and the large deformations were localized to a segement as seen in Figure 9. A closer

inspection of the collapased insert showed that cracks had propagated in this region and severed the webs. This combination of large plastic deformation and crack growth was not modelled.

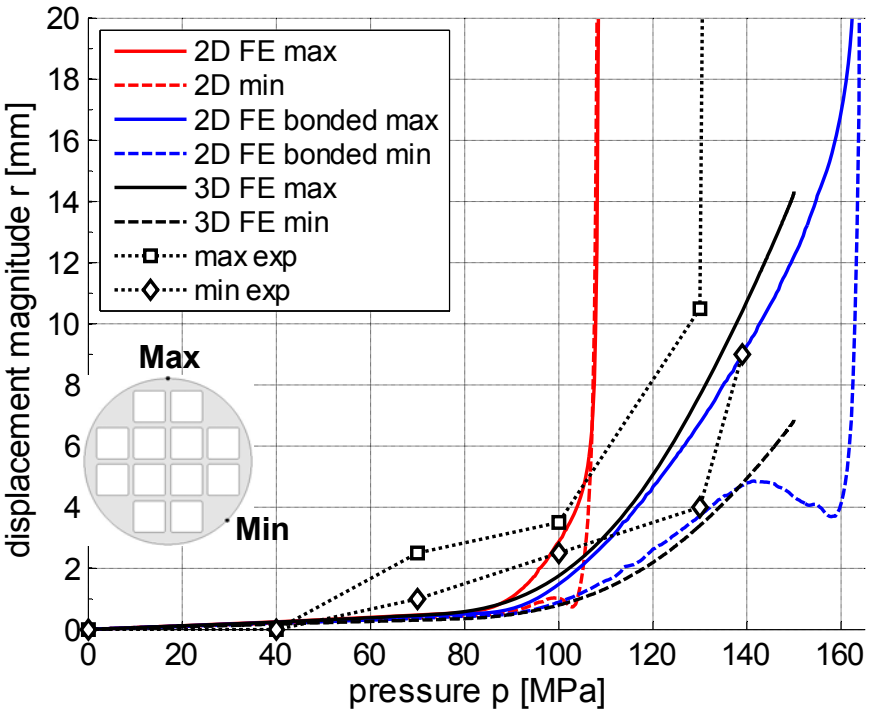

Figure 38: Displacement vs. pressure for Mock-up 2 measured and computed values at the location with the smallest and largest measured values. Max and Min indicates the locations at which the displacements were evaluated.

6. Discussion

The design load for the iso-static ice-age load is 45 MPa. The two mock-up tests indicated that the failure load is about three times higher. The finite element computations presented in this report simulate the load-displacement curve of the canister relatively well. The bonding of the steel cassettes emerges as the most important factor of uncertainty for an accurate simulation of canister failure. For the plane strain model, the difference in failure load between the extreme cases with all cassettes debonded and all bonded could be as large as 50%. Normally the cassettes are bonded but some of them may debond as the load increases. The sudden collapse and reduction in the failure load is caused by the shearing mode which becomes dominant in the 2D simulation with debonded cassettes. This shearing mode failure does not occur for the 2D model with bonded cassettes or the 3D model with debonded cassettes. Moreover, in future repositories fuel bundles will be placed inside the cassettes. This will provide additional stiffening and the shearing failure can in practice be ruled out as failure mode. The finite element mesh needs to be sufficiently refined for accurate simulation of the plastic collapse. The three-dimensional models with a relatively coarse mesh required very long computational times. Thus any simulation with converged mesh refinement will require very large computational resources. It is important to point out that symmetry should not be used for instability problems. The shearing mode for instance would not occur in a symmetry model but we can also see that the 3D model, as well as the 2D models with bonded cassettes, have non-symmetric deformation.

The mock-ups were much shorter than the real canisters. The 3D models will approach the 2D models with increasing canister length. Thus, the difference between 3D and 2D models will be smaller for the 5m canister than for the 1 metre mock-ups. The failure of the canister is very complex. The post-test inspection of the two mock-ups suggests that failure may be caused by a combination of large plastic deformation and tearing of defects. This could in principle be modelled by elastic-plastic fracture mechanics provided that the size and location of the critical defects is known.

7 Conclusions

- The mock-up tests indicated that the failure load in iso-static pressure (130 – 140MPa) is three times higher than the design load (45MPa)
- The failure load can be accurately simulated by elastic-plastic finite element simulation. The two-dimensional model gives a lower failure load than a three-dimensional model.
- The bonding of the steel cassettes inside the insert provides the largest uncertainty for an accurate prediction of the failure load. A two-dimensional model with debonded cassettes collapses in a shearing mode. This load is a lower bound for the failure load but it gives still a large safety margin agaist the design load. The corner radius of the cassettes has a negligible influence oon the failure load whereas a large off-set of the steel cassettes has a moderate influence.
- A refined finite element mesh is needed for an accurate analysis of the failure load. For a three-dimensional model the computational times may then become quite significant.

8 References

[1] Hedin A., (2006), Long-term Safety for KBS-3 repositories at Forsmark and Laxmar – a first evaluation. Main Report of the SR-Can Project, SKB Technical Report TR-06-25, Swedish Nuclear Fuel and Waste Management Co

[2] Andersson C.-G.: Development of fabrication technology for copper canisters with cast inserts, SKB Technical report TR-02-07, Swedish Nuclear Fuel and Waste Management Co, 2002

[3] Werme L., *Design Premises for Canisters for Spent Nuclear Fuel*, SKB Technical Report TR-98-08, Swedish Nuclear Fuel and Waste Management Co

[4] Andersson C-G. et al., (2005), *Probabilistic analysis and material characterisation of canister inserts for spent nuclear fuel - summary report*, SKB Technical Report TR-05-17., Swedish Nuclear Fuel and Waste Management Co

[5] Nilsson K.-F. et al.: A probabilistic methodology to determine acceptance criteria and failure probabilities for the KBS-3 ductile cast iron inserts, to appear in *Nuclear Technology*.

[6] Dillström P.: Probabilistic analysis of canister inserts for spent nuclear fuel, SKB Technical report TR-05-19, Swedish Nuclear Fuel and Waste Management Co, 2005

[7] Nilsson K.-F., Burström M., Lojaj F. and Anderson C.-G.: *Failure of spent nuclear fuel canister mock-ups at issostatic pressure*, Engineering Failure Analysis, 2006

[8] Nilsson K.-F., Lofaj F. Andersson C.-G. and Burström M.: *Pressure test of two KBS-3 canister mock-ups*, SKB Technical report TR-05-18, Swedish Nuclear Fuel and Waste Management Co, 2005

[9] Minnebo P., Nilsson K.-F. and Blagoeva D.: Tensile, compression and fracture properties of thick-walled ductile cast iron components, Journal of Materials Engineering Performance

[10] ABAQUS inc.: The ABAQUS handbook version 6.6, 2006

European Commission

EUR 23224 EN – Joint Research Centre – Institute for Energy
Title:
Author(s): O. Martin, K-F Nilsson and N. Jakšić
Luxembourg: Office for Official Publications of the European Communities
2007 – 40 pp. – 21 x 29.7 cm
EUR – Scientific and Technical Research series – ISSN 1018-5593

Abstract
This report describes an in-depth finite element simulation of a spent fuel canister for geological disposal loaded in iso-static pressure until plastic collapse. The canister consists of a copper overpack and a ductile cast iron insert with steel cassettes where the spent fuel is placed. The higgly non-linear finite element analysis is based on the explicit formulation and includes large deformations, non-linear material behaviour and contact between the canister components. The analysis includes comparison between two-and three dimensional models and assessment of the different geometrical features such as corner radius of the cassette, cassette off-set, different bonding/dedonding conditions between insert and steel cassette. The analysis shows that the bonding cassette/insert has a large impact on the collapse load. Two large-scale mock-ups test that had been performed earlier are also simulated by the developed finite element models. There is a very good agreement between measured and computed deformations versus applied load and collapse load.

How to obtain EU publications

Our priced publications are available from EU Bookshop (http://bookshop.europa.eu), where you can place an order with the sales agent of your choice.

The Publications Office has a worldwide network of sales agents. You can obtain their contact details by sending a fax to (352) 29 29-42758.

The mission of the JRC is to provide customer-driven scientific and technical support for the conception, development, implementation and monitoring of EU policies. As a service of the European Commission, the JRC functions as a reference centre of science and technology for the Union. Close to the policy-making process, it serves the common interest of the Member States, while being independent of special interests, whether private or national.